# Optimal Task Offloading and Resource Allocation for C-NOMA Heterogeneous Air-Ground Integrated Power Internet of Things Networks

Peng Qin, *Member, IEEE*, Yang Fu, Xiongwen Zhao, *Senior Member, IEEE*, Kui Wu, *Senior Member, IEEE*, Jiayan Liu, and Miao Wang

***Abstract*— By combining information communication technology with power grid, the smart grid-oriented Power Internet of Things (PIoT) has become a critical technology to guarantee the safe and reliable power grid operation and improve system energy efficiency. Nevertheless, PIoT devices have only limited communication and computing resources since they are mostly deployed in remote areas that may be out of service coverage of existing terrestrial 5G networks. To overcome the resource limitation, we leverage Air-Ground Integrated C-NOMA Heterogeneous PIoT Networks (PAGIC HetNets), and study the core challenges in PAGIC HetNets. As PIoT devices are normally powered by battery, we aim at minimizing the energy consumption of PIoT devices and thoroughly investigate the problem of task offloading and resource allocation with minimal energy consumption. This problem belongs to a mixed integer nonlinear programming (MINLP) with extra difficulty that the long-term queuing delay and short-term constraints are coupled. To tackle the difficulty, we use Lyapunov optimization to transform this hard problem into three subproblems. The first subproblem is task splitting and local computing resource assignment at the PAGIC user side, which we solve with the Lagrangian multiplier method. The second subproblem is queue-aware channel reusing, and matching theory is adopted to solve it. The third subproblem is optimizing the aerial server resource allocation, for which we propose a greedy-based solution. Numerical simulations demonstrate that our approach can obtain excellent performance in terms of energy consumption, spectrum efficiency, task backlog, and queuing delay with lower complexity compared with several benchmark methods.**

***Index Terms*— Energy minimization, air-ground integrated C-NOMA heterogeneous power-IoT networks, task offloading and resource allocation, Lyapunov optimization, matching theory, queue-awareness.**

Manuscript received 29 August 2021; revised 20 December 2021 and 5 March 2022; accepted 12 May 2022. Date of publication 24 May 2022; date of current version 11 November 2022. This work was supported in part by the Fundamental Research Funds for the Central Universities under Grant 2021MS002 and in part by the State Key Laboratory of Alternate Electrical Power System With Renewable Energy Sources under Grant LAPS21018. The associate editor coordinating the review of this article and approving it for publication was K. R. Chowdhury. *(Corresponding author: Peng Qin.)*

Peng Qin, Yang Fu, Xiongwen Zhao, Jiayan Liu, and Miao Wang are with the State Key Laboratory of Alternate Electrical Power System With Renewable Energy Sources, North China Electric Power University, Beijing 102206, China, and also with the Hebei Key Laboratory of Power Internet of Things Technology, North China Electric Power University, Baoding, Hebei 071003, China (e-mail: qinpeng@ncepu.edu.cn).

Kui Wu is with the Department of Computer Science, University of Victoria, Victoria, BC V8W 3P6, Canada (e-mail: wkui@uvic.ca).

Color versions of one or more figures in this article are available at https://doi.org/10.1109/TWC.2022.3175472.

Digital Object Identifier 10.1109/TWC.2022.3175472

## I. Introduction

SMART grid is able to provide effective solutions for distributed renewable energy and grid-connected energy storage [1]. Power Internet of Things (PIoT), which combines information communication technology (ICT) with power grid, is a prospective way to guarantee the safe and reliable power grid operation, improve system energy efficiency, and reduce greenhouse gas emission. Due to the decentralized distribution of renewable energy such as offshore wind and desert solar power, a large number of PIoT devices are deployed in remote areas, where there is commonly no information communication network coverage [2]. Moreover, as a typical type of Industrial IoT, PIoT has urgent requirements on computational and communication resources to meet the delay-sensitive and computation-intensive tasks. However, existing terrestrial 5G network is not able to supply seamless communication and reliable computational services due to inherent limitations of terrestrial 5G networks such as small coverage, fixed resource deployment, and poor emergency response capabilities [3].

As a better solution, 6G technology transforms the one-dimensional PIoT ground networks into the 3D space-air-ground heterogeneous networks, consisting of spacial component, aerial component, and ground component [4]. The spacial component consists of geostationary and low earth orbit satellites that provide wide-range communication coverage. The aerial component in composed of high altitude platform station (HAPS) and unmanned aerial vehicles (UAVs), which have a high location flexibility to provide edge computing services. The ground component consists of lots of PIoT terminals that are normally powered by battery and limited with computational capability. Within the layered infrastructure, computation tasks can be executed in the local ground component or offloaded to the spacial/aerial component for edge computing [5].

As the representative aerial segment equipment, unmanned UAVs have lower path loss and can get better line of sight (LoS) links. They could be deployed in the levitation mode. However, UAVs cannot handle scenarios that demand wide coverage, and in this case HAPSs come to rescue due to their high altitude [6]–[8]. Compared with satellites that incurs much higher cost (e.g., the construction of the Iridium system cost over 3.4 billion US dollars [9]), aerial platform-based networks with UAVs and HAPSs are regarded

as the most feasible and cost-effective solution for future 6G PIoT applications. In this paper, we introduce the Air-Ground Integrated Heterogeneous PIoT Networks (PAGI HetNets), which include one HAPS serving as a macro aerial base station to ensure wide coverage and several UAVs serving as small aerial base stations to enhance communication and computing services in remote PIoT.

In recent years, UAV communication using orthogonal multiple access (OMA), where each terminal occupies an orthogonal subchannel, has been extensively studied. Considering that the number of access terminals in future 6G network will increase exponentially, limited channels can hardly satisfy the communication requirements, and OMA is not suitable for scenarios where spectrum resources are scarce [8]. By adopting successive interference cancellation (SIC) for the receiving end, non-orthogonal multiple access (NOMA) allows more than one terminal to simultaneously use a common resource block, which can improve system throughput and spectrum utilization [10]. As the number of access terminals increases, however, the processing time in SIC increases drastically. To address this problem, Clustered-NOMA (C-NOMA), which groups HAPS's terminals into clusters, is developed to reduce the decoding complexity while ensuring system spectrum efficiency [11]. Moreover, to further improve spectrum efficiency, we also apply NOMA technique for all UAVs within the coverage of HAPS to reuse orthogonal subchannels. Based on above approach, we can guarantee the spectrum resource efficiency, while reducing the complexity of the receiving ends.

When multiple PIoT devices offload tasks to edge servers using C-NOMA in PAGI HetNets, they will cause unexpected interference, leading to serious waste of terminal energy. This is because proper subchannel assignment is vital to relieve the intra-cell and cross-cell interference to improve overall energy consumption and ensure the QoS. This problem, however, is rarely considered previously [12]. Moreover, whether processing locally or offloading to the edge and how to allocate computational resource between PIoT devices all have great influence on the subchannel assignment scheme. Last but not least, queuing delay is critical in delay-sensitive PIoT scenarios [13]. To make matters worse, the long-term constraints of queuing delay and the short-term decision making are coupled. Therefore, it is essential to cope with the coupled task offloading and resource assignment for PAGI C-NOMA HetNets bounded by queuing delay constraints.

We consider an Air-Ground Integrated C-NOMA Heterogeneous PIoT Networks (PAGIC HetNets) system, including one HAPS, multiple UAVs and a large number of PIoT devices, where HAPS uses C-NOMA, UAVs use NOMA, and all aerial base stations are equipped with edge servers. Ground PIoT users need to decide task splitting and local computing resources allocation, HAPS serve its users (called HAUs) for task offloading, and each UAV reuses spectrum resource to serve its users (called UAUs). The edge servers on both HAPS and UAVs need to optimize the sub-channel reusing scheme and allocate computing resources. Our target is minimizing the total energy consumption of PIoT terminals under the long-term queuing delay requirements. This problem is extremely to solve, due to the strong coupling of subchannel allocation, power control, and the long-term queueing delay constraints. We adopt Lyapunov optimization to decouple the short-term decision making and the long-term queuing delay constraints and decompose the optimization problem into three sub-problems: (1) task splitting and local computing resource optimization for user side, (2) channel reusing optimization, and (3) aerial edge resource assignment for the server side. We develop efficient solutions for each sub-problem and perform simulation to evaluate the performance of the whole system. Our approach can effectively address the fundamental problems for remote PIoT networks, such as low power, massive connectivity, and broad coverage [14].

The contributions of the paper are as follows.

- We propose a PAGIC HetNets system model for air-ground integrated heterogeneous PIoT networks, which consist of HAPS, UAVs, and ground PIoT devices. For PAGIC HetNets, each subchannel of HAPS is occupied by a cluster of HAUs and can be reused by more than one UAV employing NOMA. Moreover, each task of terminal can be split, which is either executed at local device or offloaded to aerial server. We formulate an energy minimization queue-aware resource allocation problem by simultaneously considering task splitting, computational resource allocation at both the user and aerial edge sides, and subchannel reusing.
- To solve the above challenging problem, we utilize Lyapunov optimization to decouple the original problem into three subproblems. The first one is the joint task splitting and local computing resource assignment for PAGIC users, which is solved by Lagrangian multiplier method. The second one is channel reusing, for which we leverage many-to-one matching optimize subchannel assignment. The third one is edge resource allocation at the server side, for which we develop a greedy algorithm. Our proposed approach achieves queue awareness by dynamically changing offloading and allocation strategies on the basis of real-time queue information.
- We conduct numerous simulations to compare our approach to several benchmark methods. Extensive simulation results demonstrate that our solution has lower complexity and can achieve superior performance in terms of energy consumption, spectrum efficiency, task backlog, and queuing delay. Simulations also verify that the proposed approach can balance the tradeoff between energy consumption and queuing delay.

For ease reference, the acronyms and main notations are listed in Table I.

The rest of the paper is organized based on the following arrangement. Related work is introduced in Section II. Section III describes system model of PAGIC HetNets. Problem formulation and decomposition based on principle of Lyapunov optimization are given in Section IV. Section V provides solution for each sub-problem. Section VI includes performance evaluation results, and Section VII concludes the paper.

TABLE I
ACRONYMS AND NOTATIONS

| Acronym/Notations | Explanation |
|---|---|
| PIoT | power Internet-of-Things |
| HAPS | high altitude platform station |
| UAV | unmanned aerial vehicle |
| C-NOMA | clustered-NOMA |
| PAGIC HetNets | air-ground integrated C-NOMA heterogeneous PIoT networks |
| HAU | HAPS user |
| UAU | UAV user |
| TSCRA | Algorithm 1: Energy minimization Task Splitting and local Computational Resource Allocation algorithm |
| EMCAM$^2$ | Algorithm 2: Energy Minimization Channel-reusing Algorithm using Many-to-one Matching |
| EMGERA | Algorithm 3: Energy Minimization Greedy based Edge Resource Allocation algorithm |
| $K$ | number of UAVs |
| $Y$ | number of PIoT users |
| $M$ | number of clusters served by HAPS |
| $B$ | number of users in a cluster |
| $N$ | number of users served by a UAV |
| $T$ | total number of time slots |
| $x_k^m(t)$ | indictor of spectrum reusing whether UAV $k$ reuses the $m$th spectrum |
| $q_m^{max}$ | maximum number of UAVs for reusing resource block/subchannel $m$ |
| $a_y^k(t)$ | indicator of task offloading whether user $U_y$ offloads tasks to the $k$th edge server |
| $R_{b,0}^m(t)/R_{n,k}^m(t)$ | uplink data rate of HAU/UAU |
| $Q_y^{loc}(t)/Q_y^{off}(t)/G_{y,k}(t)$ | backlog of local computing queue/task offloading queue/edge computing queue |
| $\Delta_V L[\Theta(t)]$ | Lyapunov drift plus penalty |
| $E(t)$ | average energy consumption in the $t$th time slot |
| $f_y(t)/f_{y,k}(t)$ | the allocated CPU-cycle frequency of user/edge server |
| $\tau_{y,max}^{Q,off}/\tau_{y,max}^{Q,loc}/\tau_{y,k,max}^{G}$ | limitation of the average queue delay |
| $Z_y^{Q,loc}(t)/Z_y^{Q,off}(t)/Z_{y,k}^{G}(t)$ | virtual queues constructed by user local computing queue/ user task offloading queue/ edge server computing queue |

## II. RELATED WORK

The space-air-ground integrated network (SAGIN) is the recent development for communication networks. Paper [15] developed a system architecture containing UAVs equipped with monostatic MIMO radars and proposed a novel sparse reconstruction algorithm to achieve accurate marine target position in SAGIN. The authors of [16] studied a framework of edge computing-enabled SAGIN to support the vehicles in remote areas. An offloading and caching algorithm was proposed to achieve real-time decision making. A task scheduling problem in SAGIN for delay-sensitive service is investigated in paper [17], and the authors designed a scheduling strategy to minimize task delay given UAV power constraint. Paper [18] introduced a joint coordinate descent optimization of users' association, power control, resource allocation, and UAV position and solved an energy minimization problem in air–ground-integrated networks. Literature [19] studied the optimal joint trajectory and resource allocation design for solar-powered multicarrier-UAV communication systems, and the low-complexity online algorithm based on successive convex optimization was developed to obtain the best resource allocation policy. Different from the above work, we present the air-ground integrated system model which does not include satellites. At the same time, HAPS and UAVs with high deployment flexibility are leveraged in the aerial segment, which can better realize the wide-range communication coverage of the ground PIoT devices.

A lot of work has studied joint resource allocation and task offloading in different scenarios. Paper [20] minimized the task completion time and energy consumption. Paper [21] designed a hierarchical genetic algorithm and particle swarm optimization-based computation approach for computation offloading. The authors of [22] investigated the resource allocation problem for NOMA-based ground networks, where the original problem was transformed into two sub-problems. A clustered multi-UAV was deployed in [23] to offer computing task offloading and resource allocation services to IoT devices, where a multi-agent deep reinforcement learning-based approach is developed to minimize the whole network computation cost under QoS requirements. Paper [24] investigated a two-hop UAV relay assisted SAGIN and solved the energy efficient resource allocation problem by optimizing channel allocation, power control, and UAV deployment iteratively. Paper [25] investigated the energy-efficient multi-task multiaccess MEC via NOMA. The authors exploited a two-step solution to effectively solve the problem of jointly optimizing task offloading, local computational resource allocation, NOMA-transmission duration and edge server task assignment. Nevertheless, none of the above work considers the long-term queue delay constraints.

The advantages of NOMA and C-NOMA over OMA have been investigated in recent years [26]. Analytical results in [27] demonstrated that compared to OMA, NOMA could efficiently decrease the energy consumption and latency of task offloading. Paper [28] developed a joint optimization framework for NOMA-enabled smallcell network (SCNet) and aimed to simultaneously maximize the sum-capacity and minimize the total power of the SCNet with co-channel interference. Energy efficiency of the C-OMA scheme was analyzed in [29], and the authors developed greedy-based C-OMA and C-NOMA, as well as joint C-OMA and C-NOMA schemes for cooperative wireless backhaul. To leverage NOMA in the context of narrow band-IoT, the authors of [30] proposed a power domain NOMA scheme with user clustering and maximized the network total throughput. Paper [31] investigated an integrated decision of user clustering and power control in downlink hybrid NOMA network and proposed two different schemes for time slot allocation. Paper [32] studied a resource allocation problem in networks composed of NOMA mobile user (MU) clusters, which considered MU fairness into transmission rate. Inspired by all the above research, we combine SAGIN with C-NOMA to obtain higher spectrum utilization.

Matching game is an effective tool for studying the resource allocation problem in communication networks [33]. To study the cooperation behaviors of cellular users and D2D pairs, paper [34] formulated the pairing problem as a matching game and transmission between CUs and D2D pairs was allowed to improve the system performance. Paper [35] minimized the latency for multitask federated learning in a

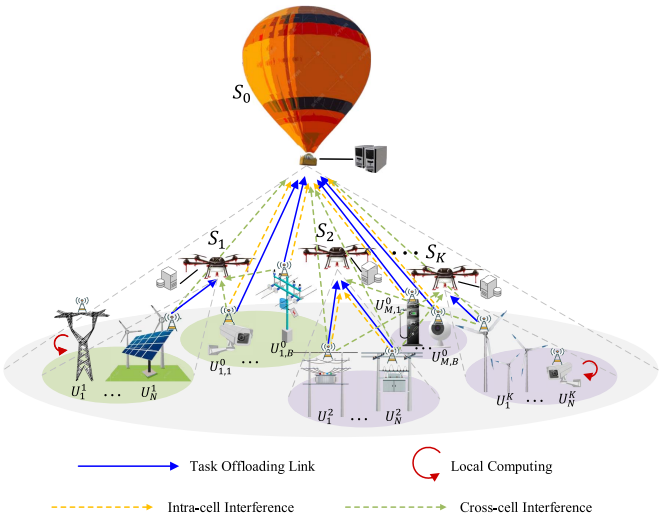


Fig. 1. The system model.

multi-access edge computing network scenario. Considering that the preference list was incomplete, the problem was addressed by an algorithm for large-scale matching. Paper [36] utilized many-to-one matching to describe the channel reusing strategy in vehicular networks and then maximized system energy efficiency under QoS constraints. Motivated by the above works, we utilize matching game to formulate and address the channel reusing MINLP problem in PAGIC HetNets.

## III. System Model

We consider an air-ground integrated PAGIC HetNets system model providing wide-range communication coverage and computation services to PIoT terminals in remote areas like deserts. As shown in Fig. 1, PAGIC HetNets system is composed of one HAPS, multiple UAVs and a large number of PIoT devices. The HAPS equipped with an edge server is deployed on demand in hovering mode and serves as a macro aerial base station to ensure wide coverage. There are totally $K$ UAVs as small aerial base stations equipped with edge servers to strengthen communication and computing service in hotpots. Since each UAV has limited coverage range, it only serves its own associated users. UAVs are also deployed in hovering mode, and their altitude and horizontal position can be optimized according to the distribution of terminal association, which, however, is out of the scope of this paper and has been solved by previous work. We use set $\mathcal{S} = \{S_0, S_1, \ldots, S_k, \ldots S_K\}$ to represent all aerial base stations, where $S_0$ corresponds to HAPS ($k = 0$) and $\{S_1, S_1, \ldots, S_k, \ldots S_K\}$ correspond to $K$ UAVs. A total of $Y$ PIoT users denoted by $\mathcal{U} = \{U_1, \ldots, U_y, \ldots, U_Y\}$ are categorized by HAUs and UAUs according to their associated base stations. Assume that there are $M$ clusters belonging to the HAPS denoted by $\mathcal{U}^0 = \{\mathcal{U}^0_1, \ldots, \mathcal{U}^0_m, \ldots, \mathcal{U}^0_M\}$ and $B$ users in cluster $\mathcal{U}^0_m = \{U^0_{m,1}, \ldots, U^0_{m,b}, \ldots, U^0_{m,B}\}$. User sets served by $K$ UAVs are respectively denoted by $\mathcal{U}^1, \ldots, \mathcal{U}^k, \ldots, \mathcal{U}^K$, where the number of users served by each UAV is $N$, that is, $\mathcal{U}^k = \{U^k_1, \ldots, U^k_n, \ldots, U^k_N\}$. Then, the whole user set is denoted by $\mathcal{U} = \mathcal{U}^0 \cup \mathcal{U}^1 \cup \ldots \cup \mathcal{U}^K$ and $Y = M \times B + K \times N$.

The $M$ clusters occupy $M$ orthogonal channels denoted by $\mathcal{C} = \{C_1, \ldots, C_m, \ldots, C_M\}$ to offload tasks to $S_0$. $B$ HAUs in each cluster use NOMA to share the channel. To improve spectrum efficiency, multiple UAVs can reuse one channel in $\mathcal{C}$ to serve UAUs. We define the channel reusing indicator $x^m_k(t) = \{0, 1\}$ to indicate the occupancy relationship between the UAV $S_k$ and the orthogonal channel $C_m$ at time $t$, i.e., $x^m_k(t) = 1$ means $S_k$ reuses $C_m$ in the $t$th time slot; otherwise $x^m_k(t) = 0$. For restricting the cross-cell interference, $q^{max}_m$ is used to denote the number of upper bound for UAVs that are allowed to occupy a common spectrum resource, constrained by $\sum_{k=1}^{K} x^m_k(t) \leqslant q^{max}_m$. The channel reusing strategy is represented by $\mathbf{x(t)} = \{x^m_k(t) \mid m = 1, \ldots, M, k = 1, \ldots, K\}$. A binary offloading indictor $a^k_y(t) = \{0, 1\}$ is introduced to represent the offloading decision from $\mathcal{U}$ to $\mathcal{S}$ in time slot $t$, i.e., $a^k_y(t) = 1$ means user $U_y$ offloads task in the $t$th time slot; otherwise $a^k_y(t) = 0$. Specifically, the offloading indictor for HAUs and UAUs can be further written as $a^k_n(t)$ and $a^0_{m,b}(t)$, respectively. For each arriving task, users can either execute locally, as shown by the red lines in Fig. 1, or offload to edge aerial server, as shown by the blue lines in Fig. 1.

We adopt a time-slotted model to formulate the optimization time period, which is evenly divided into $T$ time slots. Therefore, the duration of each time slot is $\tau$ and the entire optimization time can be expressed by $\{1, \ldots, t, \ldots, T\}$. According to [13], the model can be considered as the quasi-static process, which means that system environment maintains stable in a slot but may vary over multiple slots. Since this paper does not focus on UAV's location optimization, we only briefly illustrate the main idea. Given variables of a UAV's altitude $d$, and the horizontal and vertical coordinate $(x, y)$, the optimization of $(x, y)$ can be solved by SCA (Successive Convex Approximation) optimization or two-dimensional exhaustive search approach. Similarly, we can further optimize UAV's hovering altitude with DC (Difference of Convex) programming to obtain the optimal $d$. More details can be found in [37] and [38].

### A. Model of Communication

In this part, we present the communication model when PIoT devices offload tasks to HAPS/UAVs by taking line-of-sight (LoS), non-LoS (NLoS) paths between UAV and users and the interference into consideration.

*1) Communication Model of HAUs:* For HAU-HAPS communication [13], [39], the path loss between $U^0_{m,b}$ and $S_0$ is

$$L^m_{b,0} = 20\log_{10}\left(\frac{4\pi f_c\sqrt{d_0^2 + r^2_{b,0}}}{c}\right) + p^{LoS}_{b,0}\eta^{LoS}_{b,0} + (1 - p^{LoS}_{b,0})\eta^{NLoS}_{b,0} \quad (1)$$

where $d_0$ represents the altitude of HAPS, and $r_{b,0}$ represents the horizontal distance between $U^0_{m,b}$ and $S_0$. $\eta^{LoS}_{b,0}$ and $\eta^{NLoS}_{b,0}$ represent the additive loss of free space for LoS and NLoS paths, respectively. $f_c$ and $c$ represent the carrier frequency and

the speed of light, respectively. $p_{b,0}^{LoS}$ is the LoS probability for HAU-HAPS link, calculated with Equation (2):

$$p_{b,0}^{LoS} = \frac{1}{1+\rho_1 \exp\{-\rho_2[\tan^{-1}(\frac{d_0}{r_{b,0}}) - \rho_1]\}} \tag{2}$$

where the values of $\rho_1, \rho_2, \eta_{b,0}^{LoS}$ and $\eta_{b,0}^{NLoS}$ are selected according to the environment. The offloading interference among HAUs consists of the intra-cell interference due to NOMA and the cross-cell interference from other terminals reusing the subchannel. By using SIC technology at UAVs and the HAPS, signals from terminals sharing the same subchannel can be decoded. When applying SIC, HAPS first treats signals of other terminals as interference, and decodes signal that has the highest channel gain. After that, the signal with the highest channel gain is excluded from the interference of other terminals [40]. Without loss of generality, we define the channel gain is $g_{b,0}^m = 10^{-\frac{L_{b,0}^m}{10}}$. For the HAUs served by HAPS on subchannel $C_m$, we assume their channel gains follow the order of $g_{1,0}^m > g_{2,0}^m \cdots > g_{B,0}^m$ and the decoding order of HAUs is $U_{m,1}^0, U_{m,2}^0, \ldots, U_{m,B}^0$. Thus, the signal-to-interference-plus-noise-ratio (SINR) of HAU $U_{m,b}^0$ is calculated by Equation (3), shown at the bottom of the next page, where $\sum_{i=b+1}^{B} a_{m,i}^0(t) P_{i,0}^m 10^{-\frac{L_{i,0}^m}{10}}$ is the intra-cell interference and $\sum_{k=1}^{K} x_k^m(t) \sum_{n=1}^{N} a_n^k(t) P_{n,k}^m 10^{-\frac{L_{n,0}^m}{10}}$ is the cross-cell interference shown by the yellow and green line in Fig. 1, respectively. $P_{b,0}^m$, $P_{n,k}^m$ and $\sigma^2$ are the transmission power of HAU, the transmission power of UAU, and the noise, respectively. $L_{n,0}^m$ is the path loss of $U_n^k$ reusing the channel $C_m$, calculated with Equation (4)

$$L_{b,0}^m = 20\log_{10}\left(\frac{4\pi f_c \sqrt{d_0^2 + r_{n,0}^2}}{c}\right) + p_{n,0}^{LoS}\eta_{n,0}^{LoS} + (1 - p_{n,0}^{LoS})\eta_{n,0}^{NLoS}, \tag{4}$$

where $p_{n,0}^{LoS}$ can be calculated in the same way according to Equation (2) by substituting $d_0$ and $r_{n,0}$. As a result, the transmission rate of $U_{m,b}^0$ can be calculated by

$$R_{b,0}^m(t) = B_{b,0}^m \log_2[1 + \gamma_{b,0}^m(t)] \tag{5}$$

where $B_{b,0}^m$ is the subchannel bandwidth.

*2) Communication Model of UAUs:* Similarly, the SINR of the $n$-th decoded UAU $U_n^k$ associated with UAV $S_k$ reusing channel $C_m$ can be calculated by Equation (6), shown at the bottom of the next page, where $\sum_{i=n+1}^{N} a_i^k(t) P_{i,k}^m 10^{-\frac{L_{i,k}^m}{10}}$ is the intra-cell interference, $\sum_{m=1}^{M} x_k^m(t) \sum_{b=1}^{B} a_{m,b}^0(t) P_{b,0}^m 10^{-\frac{L_{b,0}^m}{10}} + \sum_{j=1,j\neq k}^{K} x_j^m(t) \sum_{u=1}^{N} a_u^j(t) P_{u,j}^m 10^{-\frac{L_{u,j}^m}{10}}$ is the cross-cell interference, and $P_{n,k}^m$ is power of $U_n^k$. Path loss $L_{n,k}^m$ can be calculated by

$$L_{n,k}^m = 20\log_{10}\left(\frac{4\pi f_c \sqrt{d_k^2 + r_{n,k}^2}}{c}\right) + p_{n,k}^{LoS}\eta_{n,k}^{LoS} + (1 - p_{n,k}^{LoS})\eta_{n,k}^{NLoS} \tag{7}$$

Therefore, the transmission rate of $U_n^k$ is expressed as

$$R_{n,k}^m(t) = B_{n,k}^m \log_2[1 + \gamma_{n,k}^m(t)] \tag{8}$$

where $B_{n,k}^m$ is the subchannel bandwidth.

### B. Task Queue Model

In this section, we introduce the data-partition model, where each arriving task of ground PIoT user is divided into multiple subtasks with data size equal to $A_0$ (in bits) [41]. Each subtask is either executed locally or offloaded to the aerial edge server. For each user $U_y$, the amount of arriving tasks in the $t$th time slot is $A_y(t)$, which we split into local computing tasks $A_y^{loc}(t)$ and offloading tasks $A_y^{off}(t)$. Therefore, the task splitting of $U_y$ can be expressed as

$$\begin{aligned} A_y(t) &= A_y^{loc}(t) + A_y^{off}(t) \\ A_y^{loc}(t), A_y^{off}(t) &= r \times A_0, \quad r \in \{0, 1, 2, \ldots\} \end{aligned} \tag{9}$$

Assume that there are two buffer queues for storing local computing tasks and offloading tasks at each PIoT terminal. The backlogs of these two queues in slot $t$ are denoted by $Q_y^{loc}(t)$ and $Q_y^{off}(t)$, respectively. They are calculated by formula (10) and (11), respectively.

$$Q_y^{loc}(t+1) = \{Q_y^{loc}(t) - W_y^{loc}(t)\}^+ + A_y^{loc}(t) \tag{10}$$

$$Q_y^{off}(t+1) = \{Q_y^{off}(t) - W_y^{off}(t)\}^+ + A_y^{off}(t) \tag{11}$$

where $\{h\}^+$ is an indicator function, i.e., when $h \geq 0$, $\{h\}^+ = h$; otherwise $\{h\}^+ = 0$. $W_y^{loc}(t)$ and $W_y^{off}(t)$ are the amounts of tasks that have been processed by local computing and task offloading, respectively, and have left the respective buffer queues in the $t$-th time slot. Specifically, $W_{m,b}^{off}(t)$ and $W_{k,n}^{off}(t)$ denote the task amounts leaving the offloading queue of HAUs $U_{m,b}^0$ and the offloading queue of UAUs $U_n^k$, respectively.

$$W_{m,b}^{off}(t) = \min\{Q_{m,b}^{off}(t), \tau R_{b,0}^m(t)\} \tag{12}$$

$$W_{k,n}^{off}(t) = \min\{Q_{k,n}^{off}(t), \tau R_{k,n}^m(t)\} \tag{13}$$

### C. Computation Model

In this subsection, we present computation models for both PIoT devices' local computing and aerial servers' edge computing.

*1) PIoT Devices' Local Computing:* The amount of tasks processed by $U_y$ locally in slot $t$ is calculated by

$$W_y^{loc}(t) = \min\left\{Q_y^{loc}(t), \frac{\tau f_y(t)}{\lambda_y}\right\} \tag{14}$$

where $f_y(t)$ denotes CPU frequency assigned at terminal $U_y$, and $\lambda_y$ represents required computational density (cycles/bit).

Therefore, the energy consumption of PIoT user $U_y$ for local computing in slot $t$ can be calculated by

$$E_y^{loc}(t) = \kappa[f_y(t)]^3 \min\left\{\frac{\lambda_y Q_y^{loc}(t)}{f_y(t)}, \tau\right\} \tag{15}$$

where $\kappa$ refers to the computation power parameter depending on the chip architecture [40]. Note that $E_y^{loc}(t) = E_{m,b}^{loc}(t)$ if user $U_y$ is HAU $U_{m,b}^0$, and $E_y^{loc}(t) = E_{k,n}^{loc}(t)$, if user $U_y$ is UAU $U_n^k$.

*2) Aerial Servers' Edge Computing:* For aerial edge computing server, i.e., HAPS and UAVs, the arriving task buffer queue can be established in the same way. Assume that the queue backlog where aerial server $S_k$ stores tasks offloaded from terminal $U_y$ is $G_{y,k}(t)$ in slot $t$. We have

$$G_{y,k}(t+1) = \{G_{y,k}(t) - W_{y,k}^{com}(t)\}^{+} + W_{y}^{off}(t) \quad (16)$$

$$W_{y,k}^{com}(t) = \min\left\{G_{y,k}(t), \frac{\tau f_{y,k}(t)}{\lambda_y}\right\} \quad (17)$$

where $W_{y,k}^{com}(t)$ denotes the amount of tasks offloaded from $U_y$ and executed by $S_k$, and $f_{y,k}(t)$ is the assigned computing resource for executing offloaded tasks within time slot $t$.

Thus, the energy consumption of PIoT user $U_y$ for offloading to UAV in slot $t$ is calculated by

$$E_{k,n}^{off}(t) = P_{n,k}^{m} \min\left\{\frac{Q_{k,n}^{off}(t)}{R_{n,k}^{m}(t)}, \tau\right\} \quad (18)$$

Similarly, the energy consumption of PIoT user $U_y$ for offloading to HAPS in slot $t$ can be calculated by

$$E_{m,b}^{off}(t) = P_{b,0}^{m} \min\left\{\frac{Q_{m,b}^{off}(t)}{R_{m,b}^{m}(t)}, \tau\right\} \quad (19)$$

## IV. Problem Formulation and Decomposition

We formulate an optimization problem of minimizing the total energy consumption for PIoT terminals in PAGIC HetNets satisfying the long-term queuing delay constraints.

### A. Problem Formulation

The total energy consumption $E(t)$ for PIoT users within time slot $t$ includes the energy consumption of all HAUs and UAUs for both local computing and task offloading, which is calculated by Formula (20).

$$\begin{aligned} E(t) &= \sum_{y=1}^{Y}\{a_y^k(t)\ E_y^{off}(t) + [1-a_y^k(t)]E_y^{loc}(t)\} \\ &= \sum_{m=1}^{M}\sum_{b=1}^{B}\{a_{m,b}^0(t)\ E_{m,b}^{off}(t) + [1-a_{m,b}^0(t)]E_{m,b}^{loc}(t)\} \\ &\quad + \sum_{k=1}^{K}\sum_{n=1}^{N}\{a_n^k(t)\ E_{k,n}^{off}(t) + [1-a_n^k(t)]E_{k,n}^{loc}(t)\} \end{aligned} \quad (20)$$

Therefore, the problem is for minimizing long-term average overall power consumption under the constraints of task splitting, offloading, computing resource assignment, sub-channel reusing and long-term queuing delay.

$$\begin{aligned} \mathbf{P1}: \min_{\mathbf{A^{loc}(t)},\mathbf{A^{off}(t)},\mathbf{f(t)},\mathbf{a(t)},\mathbf{x(t)}} & \lim_{T\to\infty}\frac{1}{T}\sum_{t=1}^{T}E(t) \\ \text{s.t.}\quad & C_1: a_y^k(t) = \{0,1\}, \quad \forall S_k \in \mathcal{S}, U_y \in \mathcal{U}, \\ & C_2: x_k^m(t) = \{0,1\}, \quad \forall S_k \in \mathcal{S}, C_m \in \mathcal{C}, \\ & C_3: \sum_{m=1}^{M} x_k^m(t) \leqslant 1, \quad \forall S_k \in \mathcal{S}, C_m \in \mathcal{C}, \\ & C_4: \sum_{k=1}^{K} x_k^m(t) \leqslant q_m^{max}, \quad \forall S_k \in \mathcal{S}, C_m \in \mathcal{C}, \\ & C_5: A_y(t) = A_y^{loc}(t) + A_y^{off}(t), \\ & \quad A_y^{loc}(t), A_y^{off}(t) = r \times A_0, \quad r \in \{0,1,2,\ldots\}, \\ & C_6: f_y(t) \leqslant f_{y,max}, \quad \forall U_y \in \mathcal{U}, \\ & C_7: \sum_{y=1}^{Y} f_{y,k}(t) \leqslant f_{k,max}, \quad \forall S_k \in \mathcal{S}, U_y \in \mathcal{U}, \\ & C_8: R_{b,0}^m(t) \geqslant R_{b,0,min}^m, \quad \forall U_{m,b}^0 \in \mathcal{U}^0, \\ & C_9: R_{n,k}^m(t) \geqslant R_{n,k,min}^m, \quad \forall U_{n,k}^0 \in \mathcal{U}^k, \\ & C_{10}: \lim_{T\to\infty}\frac{1}{T}\sum_{t=1}^{T}\frac{Q_y^{off}(t)}{\bar{A}_y^{off}(t)} \leqslant \tau_{y,max}^{Q,off}, \quad \forall U_y \in \mathcal{U}, \\ & C_{11}: \lim_{T\to\infty}\frac{1}{T}\sum_{t=1}^{T}\frac{Q_y^{loc}(t)}{\bar{A}_y^{loc}(t)} \leqslant \tau_{y,max}^{Q,loc}, \quad \forall U_y \in \mathcal{U}, \\ & C_{12}: \lim_{T\to\infty}\frac{1}{T}\sum_{t=1}^{T}\frac{G_{y,k}(t)}{\bar{W}_y^{off}(t)} \leqslant \tau_{y,k,max}^{G}, \\ & \forall S_k \in \mathcal{S}, \quad U_y \in \mathcal{U}, \end{aligned} \quad (21)$$

where $\mathbf{A^{loc}(t)} = \{A_y^{loc}(t), \forall U_y \in \mathcal{U}\}$ and $\mathbf{A^{off}(t)} = \{A_y^{off}(t), \forall U_y \in \mathcal{U}\}$ denote the task splitting of PIoT user $U_y$, $\mathbf{f(t)} = \{f_y(t), f_{y,k}(t), \forall S_k \in \mathcal{S}, U_y \in \mathcal{U}\}$ represents computing resource allocation, $\mathbf{a(t)} = \{a_y^k(t), \forall S_k \in \mathcal{S}, U_y \in \mathcal{U}\}$ denotes user's task offloading decision, and $\mathbf{x(t)} = \{x_k^m(t)\}$ is the channel reusing strategy. Constrains $C_1$ and $C_2$ mean that the indicators of channel reusing and task offloading are both binary variables. $C_3$ and $C_4$ mean that $q_m^{max}$ UAVs can be matched with one orthogonal channel, but one UAV can only reuse at most one orthogonal channel. $C_5$ represents task splitting constraints. $C_6$ and $C_7$ specify the computing

$$\gamma_{b,0}^m(t) = \frac{P_{b,0}^m 10^{-\frac{L_{b,0}^m}{10}}}{\sum_{i=b+1}^{B} a_{m,i}^0(t) P_{i,0}^m 10^{-\frac{L_{i,0}^m}{10}} + \sum_{k=1}^{K} x_k^m(t) \sum_{n=1}^{N} a_n^k(t) P_{n,k}^m 10^{-\frac{L_{n,0}^m}{10}} + \sigma^2} \quad (3)$$

$$\gamma_{n,k}^m(t) = \frac{P_{n,k}^m 10^{-\frac{L_{n,k}^m}{10}}}{\sum_{i=n+1}^{N} a_i^k(t) P_{i,k}^m 10^{-\frac{L_{i,k}^m}{10}} + \sum_{m=1}^{M} x_k^m(t) \sum_{b=1}^{B} a_{m,b}^0(t) P_{b,0}^m 10^{-\frac{L_{b,0}^m}{10}} + \sum_{j=1,j\neq k}^{K} x_j^m(t) \sum_{u=1}^{N} a_u^j(t) P_{u,j}^m 10^{-\frac{L_{u,j}^m}{10}}} \quad (6)$$

resource constraints for PIoT users and edge servers. $C_8$ and $C_9$ are constraints of system QoS. $C_{10} \sim C_{12}$ are the long-term queuing delay constraints. The end-to-end queuing delay mainly includes the data offloading queuing delay and the computation queuing delay. Note that the result feedback delay can be neglected because the size for computation results is generally much smaller [42].

*1) Data Offloading Queuing Delay:* According to the Little's Law, the average data offloading queuing delay is proportional to the average queue length divided by the average task arriving rate [13]. Therefore, we obtain $C_{10}$. Its right side $\tau_{y,max}^{Q,off}$ denotes the upper bound for data offloading queuing delay, and $\bar{A}_y^{off}(t)$ represents the average task arrival rate calculated by (22).

$$\bar{A}_y^{off}(t) = \frac{1}{t}\sum_{i=0}^{t-1} A_y^{off}(i) \tag{22}$$

*2) Computation Queuing Delay:* Similarly to the data offloading queuing delay, the queuing delay of local computation and aerial server computation corresponding to $Q_y^{loc}(t)$ and $G_{y,k}(t)$ can be expressed as $C_{11}$ and $C_{12}$, respectively. $\tau_{y,max}^{Q,loc}$ and $\tau_{y,k,max}^{G}$ are the upper bounds, where the average task arrival rate $\bar{A}_y^{loc}(t)$ and $\bar{W}_y^{off}(t)$ are calculated by

$$\bar{A}_y^{loc}(t) = \frac{1}{t}\sum_{i=0}^{t-1} A_y^{loc}(i) \tag{23}$$

$$\bar{W}_y^{off}(t) = \frac{1}{t}\sum_{i=0}^{t-1} a_y^k(i) W_y^{off}(i) \tag{24}$$

### *B. Lyapunov Optimization*

Note that the decision making is coupled with queuing delay constraints, making Problem **P1** extremely hard to solve. Thus, we apply Lyapunov optimization to convert the long-term issue to a series of short-term subproblems. We introduce the virtual queue concept [43] and transform $C_8 \sim C_{10}$ into queue stability constraints. Three new virtual queues corresponding to the local computing queue, the task offloading queue, and the aerial server computing queue, respectively, are proposed as follows.

$$Z_y^{Q,loc}(t+1) = \{Z_y^{Q,loc}(t) + \frac{Q_y^{loc}(t+1)}{\bar{A}_y^{loc}(t+1)} - \tau_{y,max}^{Q,loc}\}^+ \tag{25}$$

$$Z_y^{Q,off}(t+1) = \{Z_y^{Q,off}(t) + \frac{Q_y^{off}(t+1)}{\bar{A}_y^{off}(t+1)} - \tau_{y,max}^{Q,off}\}^+ \tag{26}$$

$$Z_{y,k}^{G}(t+1) = \{Z_{y,k}^{G}(t) + \frac{G_{y,k}(t+1)}{\bar{W}_y^{off}(t+1)} - \tau_{y,k,max}^{G}\}^+ \tag{27}$$

Based on the analysis in [44], we can conclude that if the above three virtual queues are mean rate stable, then the constraints $C_8 \sim C_{10}$ are automatically satisfied.

To solve Problem **P1**, we further introduce the set $\Theta(t) = \{Q_y^{off}(t), Q_y^{loc}(t), G_{y,k}(t), Z_y^{Q,off}(t), Z_y^{Q,loc}(t), Z_{y,k}^{G}(t)\}$. The Lyapunov function is defined as half of the sum of all queues' squares in $\Theta(t)$ [38], which is expressed as

$$L[\Theta(t)] = \frac{1}{2}\{\sum_{y=1}^{Y}[Q_y^{off}(t)^2 + Q_y^{loc}(t)^2 + G_{y,k}(t)^2 + Z_y^{Q,off}(t)^2 + Z_y^{Q,loc}(t)^2 + Z_{y,k}^{G}(t)^2]\} \tag{28}$$

The definition of Lyapunov drift is the expectation of Lyapunov function changes in adjacent slots:

$$\Delta L[\Theta(t)] = \mathbb{E}\{L[\Theta(t+1)] - L[\Theta(t)] | \Theta(t)\} \tag{29}$$

The magnitude of the Lyapunov drift $\Delta L[\Theta(t)]$ determines the change of the queue between two adjacent time slots and is necessary to assure the queue stability. To minimize PIoT users' total energy consumption while ensuring queue stability, Lyapunov drift plus penalty is defined as Lyapunov drift plus the expectation of average energy consumption multiplied by a weight parameter $V$ [13]:

$$\Delta_V L[\Theta(t)] = \Delta L[\Theta(t)] + V\mathbb{E}\{E(t)|\Theta(t)\} \tag{30}$$

where $V$ is nonnegative and is used to make a trade off between "penalty minimization" and "queue stability".

We can further derive that with every potential $\Theta(t)$ and $V \geqslant 0$, $\Delta_V L[\Theta(t)]$ is upper bounded as

$$\begin{aligned}
&\Delta_V L[\Theta(t)] \\
&\leqslant const + \sum_{y=1}^{Y}\mathbb{E}[Q_y^{loc}(t)(A_y^{loc}(t) - W_y^{loc}(t))|\Theta(t)] \\
&\quad + \sum_{y=1}^{Y}\mathbb{E}[Q_y^{off}(t)(A_y^{off}(t) - W_y^{off}(t))|\Theta(t)] \\
&\quad + \sum_{y=1}^{Y}\mathbb{E}[Z_y^{Q,loc}(t)\frac{Q_y^{loc}(t+1)}{\bar{A}_y^{loc}(t+1)} - \tau_{y,max}^{Q,loc}|\Theta(t)] \\
&\quad + \sum_{y=1}^{Y}\mathbb{E}[Z_y^{Q,off}(t)\frac{Q_y^{off}(t+1)}{\bar{A}_y^{off}(t+1)} - \tau_{y,max}^{Q,off}|\Theta(t)] \\
&\quad + \sum_{y=1}^{Y}\sum_{k=1}^{K}\mathbb{E}[G_{y,k}(t)(W_y^{off}(t) - W_{y,k}^{com}(t))|\Theta(t)] \\
&\quad + \sum_{y=1}^{Y}\sum_{k=1}^{K}\mathbb{E}[Z_{y,k}^{G}(t)\frac{G_{y,k}(t+1)}{\bar{W}_y^{off}(t+1)} - \tau_{y,k,max}^{G}|\Theta(t)] \\
&\quad + V\mathbb{E}[E(t)|\Theta(t)]
\end{aligned} \tag{31}$$

where

$$\begin{aligned}
const = \frac{1}{2}\{&\mathbb{E}[\sum_{y=1}^{Y} A_y^{loc}(t)^2 + W_y^{loc}(t)^2|\Theta(t)] \\
&+ \mathbb{E}[\sum_{y=1}^{Y} A_y^{off}(t)^2 + W_y^{off}(t)^2|\Theta(t)] \\
&+ \mathbb{E}[\sum_{y=1}^{Y}(\frac{Q_y^{loc}(t+1)}{\bar{A}_y^{loc}(t+1)} - \tau_{y,max}^{Q,loc})^2|\Theta(t)] \\
&+ \mathbb{E}[\sum_{y=1}^{Y}(\frac{Q_y^{off}(t+1)}{\bar{A}_y^{off}(t+1)} - \tau_{y,max}^{Q,off})^2|\Theta(t)]
\end{aligned}$$

$$+\mathbb{E}[\sum_{y=1}^{Y}\sum_{k=1}^{K}W_y^{off}(t)^2+W_{y,k}^{com}(t)^2|\Theta(t)]$$
$$+\mathbb{E}[\sum_{y=1}^{Y}\sum_{k=1}^{K}(\frac{G_{y,k}(t+1)}{\bar{W}_y^{off}(t+1)}-\tau_{y,k,max}^{G})^2|\Theta(t)]\}.$$

Substituting (10), (11), (16) and the following three formulas (32)-(34) into (31), we have:

$$\bar{A}_y^{loc}(t+1)=\frac{1}{t+1}[A_y^{loc}(t)+\sum_{i=0}^{t-1}A_y^{loc}(i)] \tag{32}$$

$$\bar{A}_y^{off}(t+1)=\frac{1}{t+1}[A_y^{off}(t)+\sum_{i=0}^{t-1}A_y^{off}(i)] \tag{33}$$

$$\bar{W}_y^{off}(t+1)=\frac{1}{t+1}[W_y^{off}(t)+\sum_{i=0}^{t-1}W_y^{off}(i)] \tag{34}$$

$$\begin{aligned}&\Delta_V L[\Theta(t)]\\&\leqslant const'+\sum_{y=1}^{Y}\mathbb{E}[Q_y^{loc}(t)(A_y^{loc}(t)-W_y^{loc}(t))|\Theta(t)]\\&\quad+\sum_{y=1}^{Y}\mathbb{E}[Q_y^{off}(t)(A_y^{off}(t)-W_y^{off}(t))|\Theta(t)]\\&\quad+\sum_{y=1}^{Y}\mathbb{E}[(t+1)Z_y^{Q,loc}(t)\\&\qquad\times(\frac{Q_y^{loc}(t)+A_y^{loc}(t)-W_y^{loc}(t)}{A_y^{loc}(t)+\sum_{i=0}^{t-1}A_y^{loc}(i)})|\Theta(t)]\\&\quad+\sum_{y=1}^{Y}\mathbb{E}[(t+1)Z_y^{Q,off}(t)\\&\qquad\times(\frac{Q_y^{off}(t)+A_y^{off}(t)-W_y^{off}(t)}{A_y^{off}(t)+\sum_{i=0}^{t-1}A_y^{off}(i)})|\Theta(t)]\\&\quad+\sum_{y=1}^{Y}\sum_{k=1}^{K}\mathbb{E}[G_{y,k}(t)(W_y^{off}(t)-W_{y,k}^{com}(t))|\Theta(t)]\\&\quad+\sum_{y=1}^{Y}\sum_{k=1}^{K}\mathbb{E}[(t+1)Z_{y,k}^{G}(t)\\&\qquad\times(\frac{G_{y,k}(t)+W_y^{off}(t)-W_{y,k}^{com}(t)}{W_y^{off}(t)+\sum_{i=0}^{t-1}W_y^{off}(i)})|\Theta(t)]\\&\quad+V\mathbb{E}[a_y^k(t)E_y^{off}(t)+[1-a_y^k(t)]E_y^{loc}(t)|\Theta(t)]\end{aligned} \tag{35}$$

where $const'=const-\sum_{y=1}^{Y}Z_y^{Q,loc}(t)\tau_{y,max}^{Q,loc}-\sum_{y=1}^{Y}Z_y^{Q,off}(t)\tau_{y,max}^{Q,off}-\sum_{y=1}^{Y}\sum_{k=1}^{K}Z_{y,k}^{G}(t)\tau_{y,k,max}^{G}$, and it has no concern with the Lyapunov optimization.

We need to "opportunistically" minimize the drift minus penalty in each time slot [43]. Therefore, we get the following objective function

$$\begin{aligned}&obj(t)\\&=\sum_{y=1}^{Y}\Bigg[a_y^k(t)E_y^{off}(t)+Q_y^{loc}(t)\left(A_y^{loc}(t)-\frac{\tau f_y(t)}{\lambda_y}\right)\\&\quad+Q_y^{off}(t)(A_y(t)-A_y^{loc}(t))\\&\quad+(t+1)Z_y^{Q,loc}(t)\left(\frac{Q_y^{loc}(t)+A_y^{loc}(t)-\frac{\tau f_y(t)}{\lambda_y}}{A_y^{loc}(t)+\sum_{i=0}^{t-1}A_y^{loc}(i)}\right)\\&\quad+(t+1)Z_y^{Q,off}(t)\left(\frac{Q_y^{off}(t)+A_y(t)-A_y^{loc}(t)}{A_y(t)-A_y^{loc}(t)+\sum_{i=0}^{t-1}A_y^{off}(i)}\right)\Bigg]\\&\quad+\sum_{y=1}^{Y}\sum_{k=1}^{K}\Bigg\{[1-a_y^k(t)]V[E_y^{off}(t)]+G_{y,k}(t)W_y^{off}(t)\\&\quad-Q_y^{off}(t)W_y^{off}(t)-\frac{(t+1)Z_y^{Q,off}(t)W_y^{off}(t)}{A_y^{off}(t)+\sum_{i=0}^{t-1}A_y^{off}(i)}\\&\quad+(t+1)Z_{y,k}^{G}(t)\left(\frac{G_{y,k}(t)+W_y^{off}(t)}{W_y^{off}(t)+\sum_{i=0}^{t-1}W_y^{off}(i)}\right)\\&\quad+G_{y,k}(t)\frac{\tau f_{y,k}(t)}{\lambda_y}\Bigg\}+\sum_{y=1}^{Y}\frac{(t+1)Z_{y,k}^{G}(t)+\frac{\tau f_{y,k}(t)}{\lambda_y}}{W_y^{off}(t)+\sum_{i=0}^{t-1}W_y^{off}(i)}\end{aligned} \tag{36}$$

### C. Problem Decomposition

In light of Lyapunov optimization, **P1** can be decomposed into three subproblems, which can be handled independently.

*1) Task Splitting and Local Computing Resource Assignment for Users (**SP1**):* First of all, we need to optimize the proportion of local computing and task offloading for task splitting. Then the allocated computing resource at the PIoT user side should be determined in slot $t$. Problem **SP1** is represented by

$$\begin{aligned}&\mathbf{SP1}:\\&\min_{a_y^k(t),A_{y^{loc}}^{loc}(t),A_y^{off}(t),f_y(t)}\Lambda(A_y^{loc}(t),f_y(t))\\&=V\kappa[f_y(t)]^3\min\left\{\frac{\lambda_y Q_y^{loc}(t)}{f_y(t)},\tau\right\}\\&\quad+Q_y^{loc}(t)(A_y^{loc}(t)-\frac{\tau f_y(t)}{\lambda_y})+Q_y^{off}(t)(A_y(t)-A_y^{loc}(t))\\&\quad+(t+1)Z_y^{Q,loc}(t)\left(\frac{Q_y^{loc}(t)+A_y^{loc}(t)-\frac{\tau f_y(t)}{\lambda_y}}{A_y^{loc}(t)+\sum_{i=0}^{t-1}A_y^{loc}(i)}\right)\\&\quad+(t+1)Z_y^{Q,off}(t)\left(\frac{Q_y^{off}(t)+A_y(t)-A_y^{loc}(t)}{A_y(t)-A_y^{loc}(t)+\sum_{i=0}^{t-1}A_y^{off}(i)}\right)\\&\quad\text{s.t.}\quad C_1,C_5,C_6\\&\qquad C_{13}:\frac{\tau f_y(t)}{\lambda_y}\leqslant Q_y^{loc}(t)\end{aligned} \tag{37}$$

*2) Channel Reuse and Task Offloading Optimization (**SP2**):* Channel allocation decision is optimized in **SP2** which determines how UAVs reuse the channel to serve the associated users in slot $t$. Problem **SP2** is represented by

$$\mathbf{SP2}:$$

$$\begin{aligned}&\min_{x_k^m(t)} \Psi(x_k^m(t)) = \sum_{m=1}^{M}\sum_{y=1}^{Y}\sum_{k=1}^{K} V[E_y^{off}(t)] \\ &- Q_y^{off}(t)W_y^{off}(t) - \frac{(t+1)Z_y^{Q,off}(t)W_y^{off}(t)}{A_y^{off}(t)+\sum_{i=0}^{t-1}A_y^{off}(i)} \\ &+ G_{y,k}(t)W_y^{off}(t) + Z_{y,k}^{G}(t)\frac{(t+1)(G_{y,k}(t)+W_y^{off}(t))}{W_y^{off}(t)+\sum_{i=0}^{t-1}W_y^{off}(i)} \\ &\text{s.t.}\quad C_2, C_3, C_4, C_8, C_9 \end{aligned} \tag{38}$$

*3) Edge Resource Allocation at Aerial Server Side (**SP3**):* The HAPS and UAVs servers determine the computing resource allocation to process tasks from the associated PIoT users in slot $t$. Problem **SP3** is represented by

$$\mathbf{SP3}:$$

$$\begin{aligned}&\max_{f_{y,k}(t)} \Omega(f_{y,k}(t)) \\ &= \sum_{y=1}^{Y}\left[G_{y,k}(t)\frac{\tau f_{y,k}(t)}{\lambda_y} + \frac{(t+1)Z_{y,k}^{G}(t)+\frac{\tau f_{y,k}(t)}{\lambda_y}}{W_y^{off}(t)+\sum_{i=0}^{t-1}W_y^{off}(i)}\right] \\ &\text{s.t.}\quad C_7 \\ &\quad C_{14}: \frac{\tau f_{y,k}(t)}{\lambda_{y,k}} \leqslant G_{y,k}(t)\end{aligned} \tag{39}$$

## V. Solution Algorithms of Energy-Minimization Queue-Aware Task Offloading and Resource Allocation for Pagic Hetnets

In this section, we propose solutions to the above three sub-problems. For **SP1**, the Lagrangian multiplier method is used to jointly optimize task splitting portion and local computing resource allocation at the PAGIC user side. Since **SP2** is still an NP-hard MINLP problem, we leverage matching theory to obtain the channel reusing result in a distributed manner. For **SP3**, we propose a low-complexity greedy algorithm to optimize the resource allocation at the server side. By solving the three sub-problems, we obtain the final optimization result of **P1**.

### *A. Task Splitting and Local Computing Resource Assignment of PAGIC User for **SP1***

Since the objective function $\Lambda(A_y^{loc}(t), f_y(t))$ in **SP1** is convex, we leverage Lagrange multiplier method to solve it [35]. The Lagrangian function is given by

$$\begin{aligned}&\mathcal{L}_y(A_y^{loc}(t), f_y(t), \mu_y, \theta_y) \\ &= \Lambda(A_y^{loc}(t), f_y(t)) \\ &\quad + \mu_y[f_y(t) - f_{y,max}] + \theta_y\left[\frac{\tau f_y(t)}{\lambda_y} - Q_y^{loc}(t)\right]\end{aligned} \tag{40}$$

where $\mu_y$ and $\theta_y$ represent Lagrange multipliers. According to Karush-Kuhn-Tucker (KKT) conditions, the optimal result could be achieved by setting the partial derivatives of (40) with respect to $A_y^{loc}(t)$, $f_y(t)$, $\mu_y$ and $\theta_y$ to zero:

$$\begin{cases}\dfrac{\partial \mathcal{L}_y(A_y^{loc}(t), f_y(t), \mu_y, \theta_y)}{\partial A_y^{loc}(t)} = 0 \\ \dfrac{\partial \mathcal{L}_y(A_y^{loc}(t), f_y(t), \mu_y, \theta_y)}{\partial f_y(t)} = 0 \\ \dfrac{\partial \mathcal{L}_y(A_y^{loc}(t), f_y(t), \mu_y, \theta_y)}{\partial \mu_y} = 0 \\ \dfrac{\partial \mathcal{L}_y(A_y^{loc}(t), f_y(t), \mu_y, \theta_y)}{\partial \theta_y} = 0\end{cases} \tag{41}$$

To solve the first equation of (41), $\frac{\partial \mathcal{L}_y(A_y^{loc}(t), f_y(t), \mu_y, \theta_y)}{\partial A_y^{loc}(t)} = 0$ can be transformed into

$$\begin{aligned}&[Q_y^{loc}(t) - Q_y^{off}(t)][A_y^{loc}(t) + \sum_{i=0}^{t-1}A_y^{loc}(i)]^2[A_y(t) \\ &- A_y^{loc}(t) + \sum_{i=0}^{t-1}A_y^{off}(i)]^2 + (t+1)Z_y^{Q,loc}(t)[\sum_{i=0}^{t-1}A_y^{loc}(i) \\ &- Q_y^{loc}(t) + \frac{\tau f_y(t)}{\lambda_y}][A_y(t) - A_y^{loc}(t) + \sum_{i=0}^{t-1}A_y^{off}(i)]^2 \\ &+ (t+1)Z_y^{Q,off}(t)[\sum_{i=0}^{t-1}A_y^{off}(i) \\ &+ Q_y^{off}(t)][A_y^{loc}(t) + \sum_{i=0}^{t-1}A_y^{loc}(i)]^2 = 0\end{aligned} \tag{42}$$

It can be seen that (42) is a one-variable quartic equation, which is solved using the Ferrari's method [45]. We briefly explain the principle of Ferrari's method here. First of all, (42) can be expressed in the following form.

$$A_y^{loc}(t)^4 + \varepsilon A_y^{loc}(t)^3 + \xi A_y^{loc}(t)^2 + \varsigma A_y^{loc}(t) + \sigma = 0 \tag{43}$$

where $\varepsilon$, $\xi$, $\varsigma$ and $\sigma$ are all constants. Then (43) is shifted to obtain

$$A_y^{loc}(t)^4 + \varepsilon A_y^{loc}(t)^3 = -\xi A_y^{loc}(t)^2 - \varsigma A_y^{loc}(t) - \sigma \tag{44}$$

Adding $[\frac{1}{2}\varepsilon A_y^{loc}(t)]^2$ on both sides can get

$$[A_y^{loc}(t)^2 + \frac{1}{2}\varepsilon A_y^{loc}(t)]^2 = (\frac{1}{4}\varepsilon^2 - \xi)A_y^{loc}(t)^2 - \varsigma A_y^{loc}(t) - \sigma. \tag{45}$$

By Adding $[A_y^{loc}(t)^2 + \frac{1}{2}\varepsilon A_y^{loc}(t)]\omega + \frac{1}{4}\omega^2$ on both sides, we can further derive

$$\begin{aligned}&\{[A_y^{loc}(t)^2 + \frac{1}{2}\varepsilon A_y^{loc}(t)] + \frac{1}{2}\omega\}^2 \\ &= (\frac{1}{4}\varepsilon^2 - \xi + \omega)A_y^{loc}(t)^2 + (\frac{1}{2}\varepsilon\omega - \varsigma)A_y^{loc}(t) + \frac{1}{4}\omega^2 - \sigma\end{aligned} \tag{46}$$

where $\omega$ is a newly introduced parameter. When $A_y^{loc}(t)$ is equal to the root of equation (43), the above formula holds no matter what value $\omega$ takes. If the value of $\omega$ can make the right term of (46) expressed as a complete square, then we

**Algorithm 1** Energy Minimization Task Splitting and Local Computational Resource Allocation Algorithm (TSCRA)

**Input:** $T$, $A_y(t)$, $\lambda_y$, $V$, $\kappa$, $\tau_{y,max}^{Q,off}$, $\tau_{y,max}^{Q,loc}$, $f_{y,max}$.
**Output:** $A_y^{loc*}(t)$, $f_y^*(t)$, $a_y^{k*}(t)$.
**Initialize:** $Q_y^{loc}(1) = 0$, $Q_y^{off}(1) = 0$, $Z_y^{Q,loc}(1) = 0$, $Z_y^{Q,off}(1) = 0$.
**while** $t = 1 \sim T$ **do**
  **while** $U_y \in \mathcal{U}$ **do**
    $\beta = 0$
    **while** $|A_y^{loc*}(t,\beta+1) - A_y^{loc*}(t,\beta)| \geqslant \Delta ||| f_y^*(t,\beta+1) - f_y^*(t,\beta)| \geqslant \Delta$ **do**
      obtain $A_y^{loc*}(t,\beta+1)$ by Ferrari's method
      obtain $f_y^*(t,\beta+1)$ using (48)
      update $\mu_y(t,\beta+1)$ and $\theta_y(t,\beta+1)$ using (49) and (50)
      $\beta = \beta + 1$
    **end while**
    $A_y^{loc*}(t) = A_y^{loc*}(t,\beta_{max})$ and $f_y^*(t) = f_y^*(t,\beta_{max})$
    update $Q_y^{loc}(t)$, $Q_y^{off}(t)$, $Z_y^{Q,loc}(t)$ and $Z_y^{Q,off}(t)$ using (10), (11), (25) and (26)
    **if** $A_y^{loc*}(t) == A_y(t)$ **then**
      $a_y^{k*}(t) = 0$
    **else**
      $a_y^{k*}(t) = 1$
    **end if**
  **end while**
**end while**

can obtain the final result, in which case $\omega$ needs to satisfy the following discriminant:

$$(\frac{1}{2}\varepsilon\omega - \varsigma)^2 - 4(\frac{1}{4}\varepsilon^2 - \xi + \omega)(\frac{1}{4}\omega^2 - \sigma) = 0 \tag{47}$$

This is a one-variable cubic equation of $\omega$, which can be directly solved by Kaldan's formula [45]. After getting $\omega$, (46) can be transformed into a quadratic equation and $A_y^{loc}(t)$ can be obtained directly.

The second equation of (41) $\frac{\partial \mathcal{L}_y(A_y^{loc}(t), f_y(t), \mu_y, \theta_y)}{\partial f_y(t)} = 0$ is a quadratic equation and $f_y^*(t)$ can be directly solved by (48), shown at the bottom of the next page, where $\beta$ is the loop index of Lagrangian multipliers.

The Lagrangian multiplier is updated using gradient method with Equations (49) and (50).

$$\mu_y(t,\beta+1) = \{\mu_y(t,\beta) + \zeta_{\mu_y}(t,\beta)[f_y(t,\beta) - f_{y,max}]\}^+ \tag{49}$$

$$\theta_y(t,\beta+1) = \{\theta_y(t,\beta) + \zeta_{\theta_y}(t,\beta)[\frac{\tau f_y(t,\beta)}{\lambda} - Q_y^{loc}(t)]\}^+ \tag{50}$$

where $\zeta_{\mu_y}$ and $\zeta_{\theta_y}$ are the updating step sizes, which should be set according to the convergence of the optimization.

Based on the above analysis, we propose Algorithm 1 (**TSCRA**) to solve Problem **SP1**.

### *B. Many-to-One Matching Based Channel Reusing Optimization for **SP2***

As described previously, each subchannel occupied by the HAPS can be reused by multiple UAVs. To find a tractable solution to **SP2**, we formulate the subproblem as a many-to-one matching problem with peer effects since both intra-cell interference and cross-cell interference should be taken into consideration [46]. The matching parties are the set of UAVs $\{S_1, \ldots, S_K\}$ and the set of orthogonal subchannels $\{C_1, \ldots, C_M\}$. **SP2** can be solved, when UAVs and subchannels are matched with objective of minimizing terminals' energy consumption of task offloading in slot $t$.

For each UAV $S_k$ and channel $C_m$, $\Pi$ is called a many-to-one matching if $\Pi(k) = \{m\} || k \in \Pi(m)$ such that $|\Pi(k)| = 1$ and $|\Pi(m)| \leqslant q_m^{max}$ corresponding to the constraints $C_3$ and $C_4$, where $|\Pi(*)|$ is the cardinality. Before proposing the matching based energy minimization channel-reusing algorithm, we first define the utility function for each UAV $S_k$ and resource block $C_m$ under matching $\Pi$ as follows.

Since each UAV tries to minimize energy consumption of its severed UAUs for task offloading in Problem **SP2**, UAV $S_k$'s utility function reusing channel $C_m$ can be denoted by

$$\begin{aligned}
&\Psi_k(m) \\
&= -\sum_{n=1}^{N} a_n^{k*}(t)\Bigg[VP_{n,k}^m(t)\min\left\{\frac{Q_{k,n}^{off}(t)}{R_{n,k}^m(t)}, \tau\right\} \\
&\quad + \min\{Q_{k,n}^{off}(t), \tau R_{n,k}^m(t)\}\big(G_{k,n}(t) - Q_{k,n}^{off}(t) \\
&\quad - \frac{(t+1)Z_{k,n}^{Q,off}(t)}{A_{k,n}^{off}(t) + \sum_{i=0}^{t-1} A_{k,n}^{off}(i)}\big) + (t+1)Z_{n,k}^G(t) \\
&\quad \times \big(\frac{G_{n,k}(t) + \min\{Q_{k,n}^{off}(t), \tau R_{n,k}^m(t)\}}{\min\{Q_{k,n}^{off}(t), \tau R_{n,k}^m(t)\} + \sum_{i=0}^{t-1} W_{k,n}^{off}(i)}\big)\Bigg]
\end{aligned} \tag{51}$$

Analogously, each orthogonal channel $C_m$ only concerns about the energy consumption of all users occupying $C_m$ for task offloading. Thus, channel $C_m$'s utility function under matching $\Pi$ is defined as

$$\begin{aligned}
&\Psi_m(\Pi(m)) \\
&= -\sum_{b=1}^{B} a_{m,b}^{0*}(t)\Bigg[VP_{b,0}^m(t)\min\left\{\frac{Q_{m,b}^{off}(t)}{R_{b,0}^m(t)}, \tau\right\} \\
&\quad + \min\{Q_{m,b}^{off}(t), \tau R_{b,0}^m(t)\}(G_{m,b,0}(t) - Q_{m,b}^{off}(t) \\
&\quad - \frac{(t+1)Z_{m,b}^{Q,off}(t)}{A_{m,b}^{off}(t) + \sum_{i=0}^{t-1} A_{m,b}^{off}(i)}) + (t+1)Z_{m,b,0}^G(t) \\
&\quad \times \big(\frac{G_{m,b,0}(t) + \min\{Q_{m,b}^{off}(t), \tau R_{b,0}^m(t)\}}{\min\{Q_{m,b}^{off}(t), \tau R_{b,0}^m(t)\} + \sum_{i=0}^{t-1} W_{m,b}^{off}(i)}\big)\Bigg] \\
&\quad - \sum_{j \in \Pi(m)} \sum_{n=1}^{N} a_n^{k*}(t)\Bigg[VP_{n,j}^m(t)\min\left\{\frac{Q_{j,n}^{off}(t)}{R_{n,j}^m(t)}, \tau\right\} \\
&\quad + \min\{Q_{j,n}^{off}(t), \tau R_{n,j}^m(t)\}(G_{j,n}(t) - Q_{j,n}^{off}(t) \\
&\quad - \frac{(t+1)Z_{j,n}^{Q,off}(t)}{A_{j,n}^{off}(t) + \sum_{i=0}^{t-1} A_{j,n}^{off}(i)}) + (t+1)Z_{n,j}^G(t)
\end{aligned}$$

**Algorithm 2** Energy Minimization subChannel-Reusing Algorithm Based on Many-to-One Matching (EMCAM$^2$)

**Input:** $G_{y,k}(t)$, $Q_y^{off}(t)$, $Z_y^{Q,off}(t)$, $A_y^{off}(t)$, $Z_{y,k}^{G}(t)$.
**Output:** A stable Matching $\Pi$ and channel reusing strategy $\mathbf{x(t)}$.
**Initialize:** generate an initial matching $\Pi$ randomly.
**while** $t = 1 \sim T$ **do**
  **repeat**
  **while** $S_k \in \mathcal{S}$ **do**
    **while** $S_k' \in \mathcal{S} \setminus \{S_k\}$ **do**
      obtain $\Psi_k(m)$ and $\Psi_m(\Pi(m))$ using (51) and (52)
      **if** $(S_k, S_k')$ is a blocking pair, $\Pi(k) = m$, $\Pi(k') = m'$ **then**
        $\Pi \Leftarrow \Pi_k^{k'}$
      **end if**
    **end while**
  **end while**
  **until:** no blocking pair exists
  obtain $\mathbf{x(t)}$ in slot $t$ by $\Pi$
**end while**

$$\times \left(\frac{G_{n,j}(t) + \min\{Q_{j,n}^{off}(t), \tau R_{n,j}^{m}(t)\}}{\min\{Q_{j,n}^{off}(t), \tau R_{n,j}^{m}(t)\} + \sum_{i=0}^{t-1} W_{j,n}^{off}(i)}\right)\Bigg] \quad (52)$$

It can be seen that the above two utility functions are consistent with the objective function $\Psi(x_k^m(t))$ of **SP2**. Therefore, finding an appropriate channel reusing result between the two matching parties is equivalent to solving the second subproblem.

In order to describe the preference for matching players, we define the preference relationship $\succ$ for all UAVs and orthogonal channels. For $S_k$, the preference relationship $\succ_k$ is introduced over channels as follows. For any two channels $C_m \neq C_m'$ and matchings $\Pi, \Pi'$, $\Pi(k) = m, \Pi'(k) = m'$:

$$(m, \Pi) \succ_k (m', \Pi') \Leftrightarrow \Psi_k(m) > \Psi_k(m') \quad (53)$$

It denotes that $S_k$ prefers $C_m$ to $C_m'$ if its associated users consume lower power on channel $C_m$ than on $C_m'$. Analogously, each $C_m$'s preference relationship $\succ_m$ over UAVs is defined as follows. For two subsets of UAVs $\mathcal{SC}, \mathcal{SC}' \subseteq \{1, \ldots k, \ldots, K\}$ and matchings $\Pi, \Pi', \Pi(m) = \mathcal{SC}, \Pi'(m) = \mathcal{SC}'$:

$$(\mathcal{SC}, \Pi) \succ_m (\mathcal{SC}', \Pi') \Leftrightarrow \Psi_m(\Pi(m)) > \Psi_m(\Pi'(m)) \quad (54)$$

It means that $C_m$ prefers $\mathcal{SC}$ to $\mathcal{SC}'$ if all users of $\mathcal{SC}$ consume lower power than that of $\mathcal{SC}'$ for task offloading. Motivated by the college admission issue [46], swap matching's definition is given.

*Definition 1:* A swap matching can be defined as a matching $\Pi_{k'}^{k}$ with $\Pi_{k'}^{k} = \Pi \setminus \{(S_k, C_m), (S_k', C_m')\} \cup \{(S_k, C_m'), (S_k', C_m)\}$ for a matching $\Pi$ with $k \in \Pi(m) \& k' \in \Pi(m')$, if $k' \in \Pi_{k'}^{k}(m) \& k' \notin \Pi_{k'}^{k}(m')$, and $k \in \Pi_{k'}^{k}(m') \& k \notin \Pi_{k'}^{k}(m)$.

Based on above definition, the concept of blocking pair is presented.

*Definition 2:* A pair of UAVs $(S_k, S_k')$ is known as a blocking pair for a matching $\Pi$ with $k \in \Pi(m) \& k' \in \Pi(m')$, if for a swap matching $\Pi_{k'}^{k}$, the utilities of all participants do not decrease, and at least one utility increases. A matching $\Pi$ is said to achieve stability if there is no blocking pair for $\Pi$.

In light of above definitions, we develop **EMCAM**$^2$ Algorithm 2 to achieve energy minimization channel reusing optimization on basis of many-to-one matching.

According to Definition 2, the system utility will gradually increase with swap matchings. Meanwhile, the finite number of UAVs guarantees that the number of swaps is limited. Thus, Algorithm 2 is able to achieve convergence within finite swap operations. Specifically, **EMCAM**$^2$ is queue-aware since it alters channel reusing and task offloading decisions according to the dynamic real-time queuing information. For example, when queue backlog grows too large, the queuing delay may exceed its bound which gives feedback to the utility functions. This will impact players' preferences and task offloading strategies and motivate the terminals to choose better local computing with superior queuing delay performance.

### C. Edge Resource Allocation at Aerial Server Side for *SP3*

For $\Omega(f_{y,k}(t))$ in **SP3**, we propose a greedy-based edge computing resource allocation approach at the aerial server side. Note that $S_k$ is associated with user set $\mathcal{U}^k$, where each user has an offloading task queue $G_{y,k}(t)$. If the offloading queue in slot $t$ is not empty, the corresponding user is called edge computing user. Define $\mathcal{U}_s^k(t) = \{\mathcal{U}^k | G_{y,k}(t) \neq 0\}$ as the set of edge computing users and the available edge computing resources in slot $t$ as $F_k(t)$. It is initially equal to $f_{k,max}(t)$. During the resource allocation progress, $F_k(t)$ continues to decrease. For user $U_y^k$, the maximum CPU frequency it can be allocated from aerial edge server $S_k$ is $f_{y,k,max}(t)$.

$$f_{y,k,max}(t) = \frac{\lambda_y G_{y,k}(t)}{\tau} \quad (55)$$

The following formula from target of **SP3** is then used to calculate the objective value.

$$\Omega_{y,k}(f_{y,k}(t)) = G_{y,k}(t)\frac{\tau f_{y,k}(t)}{\lambda_{k,y}} + \frac{(t+1) Z_{y,k}^{G}(t) \frac{\tau f_{y,k}(t)}{\lambda_{k,y}}}{W_{k,y}^{off}(t) + \sum_{i=0}^{t-1} W_{k,y}^{off}(i)} \quad (56)$$

The user with the maximum objective value will be chosen with the CPU-cycle frequency calculated as

$$\delta_{y,k}(t) = \min\left\{F_k(t), \frac{\lambda_y}{\tau} G_{y,k}(t)\right\} \quad (57)$$

$$f_y^*(t, \beta+1) = \sqrt{\frac{1}{3V\kappa \min\left\{\frac{\lambda_y Q_y^{loc}(t)}{f_y(t,\beta)}, \tau\right\}} \left\{\frac{Q_y^{loc}(t)\tau}{\lambda_y} + \frac{(t+1) Z_y^{Q,loc}(t)\tau}{\lambda_y [A_y^{loc}(t) + \sum_{i=0}^{t-1} A_y^{loc}(i)]} - \mu_y(t,\beta) - \theta_y(t,\beta)\frac{\tau}{\lambda_y}\right\}} \quad (48)$$

**Algorithm 3** Energy Minimization Greedy Based Edge Resource Allocation Algorithm (EMGERA)

**Input:** $G_{y,k}(t)$, $\lambda_y$, $Z^G_{y,k}(t)$, $W^{off}_y(t)$, $f_{k,max}$.
**Output:** $f^*_{y,k}(t)$.
**while** $t = 1 \sim T$ **do**
  **while** $S_k \in \mathcal{S}$ **do**
    **Initialize:** $\mathcal{U}^k_S(t) = \{\mathcal{U}^k | G_(y,k)(t) \neq 0\}$ and $F_k(t) = f_{k,max}$.
    **while** $\mathcal{U}^k_S(t) \neq \varnothing \&\& F_k(t) > 0$ **do**
      $\delta_{y,k}(t) = \min\{F_k(t), \frac{\lambda_y}{\tau} G_{y,k}(t)\}$
      obtain $\Omega_{y,k}(\delta_{y,k}(t))$ using (56)
      $U^{k*}_y = \arg[\max \Omega_{y,k}(\delta_{y,k}(t))]$
      $f^*_{y,k}(t) = \delta_{y,k}(t)$
      $\mathcal{U}^k_S(t) = \mathcal{U}^k_S(t) \setminus U^{k*}_y$
      $F_k(t) = F_k(t) - f^*_{y,k}(t)$
    **end while**
  **end while**
**end while**

The process of resource allocation will not end until all users' task offloading queues have been allocated computing resource, or the available resource $F_k(t)$ becomes zero. Details are illustrated in **EMGERA** of Algorithm 3 for aerial edge computing resource allocation.

### *D. Energy-Minimization Queue-Aware Task Offloading and Resource Allocation*

The above three algorithms solve each sub-problem step by step and form a joint task offloading and resource allocation algorithm to obtain the final energy-minimization optimization result of **P1**. In each time slot, task splitting portion and local computing resource allocation at the PAGIC user side are first obtained by Algorithm 1, channel reusing result is solved by Algorithm 2, and the resource allocation at the server side is optimized by Algorithm 3. Task queues are updated after the current slot optimization and the state transitions to the next slot. Our approach stops until $t > T$.

### *E. Properties Analyses*

In this section, we theoretically analyze the convergence, optimality and complexity of TSCRA, EMCAM$^2$ and EMGERA algorithms.

*1) Convergence:* Since **SP1** is a convex optimization problem and the number of PIoTs is limited, Algorithm 1 can obviously converge to a final result with the updating of Lagrangian multipliers. For Algorithm 2, according to many-to-one matching definitions, the target value of $\Psi_m(\Pi(m))$ continues to decrease until a stable matching result is found within finite swap operations. The edge computation resource allocation process in Algorithm 3 is also convergent because the number of UAVs and users is limited. In addition, the overall system energy consumption can also be bounded for finite computing and communication resources.

TABLE II
SIMULATION PARAMETERS

| Parameter | Value |
|---|---|
| Sum of time slots $T$ | 100 |
| Duration of a time slots $\tau$ | 0.1 s |
| UAVs's number $K$ | 4-12 |
| Number of HAU clusters/orthogonal channel $M$ | 2-12 |
| Additive loss $\eta^{LoS}_{y,k}$, $\eta^{NLoS}_{y,k}$ | 0.1, 21 |
| Carrier frequency $f_c$ | 0.1 GHz |
| Altitude of HAPS and UAVs $d_0$,$d_k$ | 150 m, 90 m |
| Noise power $\sigma^2$ | -144 dBm |
| Environment parameters $\rho_1$,$\rho_2$ | 4.88, 0.43 |
| Transmit power $P^m_{y,k}$ | 23 dBm |
| Computational density $\lambda_y$ | 1000 CPU cycles/bit |
| Queuing delay bound $\tau^{Q,off}_{y,max}$,$\tau^{Q,loc}_{y,max}$,$\tau^{G}_{y,k,max}$ | 100, 140, 50 ms |
| Computation power parameter $\kappa$ | $5\times10^{-26}$ J/Hz3/s |
| Weight parameter $V$ | $10^6$ |
| Bandwidth $B^m_{y,k}$ | 1 MHz |

*2) Optimality:* The optimized task splitting proportion and local computing resource allocation for PIoT users can be obtained by Algorithm 1. Because **SP1** is a strict convex optimization problem, we applied the KKT conditions to calculate the optimization result in each iteration. It is able to converge to the final result, which is optimal. By the swap operations of Algorithm 2, the utilities of all participants do not decrease, and at least one utility increases. Therefore, the total energy consumption of PIoT devices decreases after each operation and an approximately optimal channel allocation result can be obtained in a distributed manner. The resource allocation of aerial server can be optimized by Algorithm 3 based on the greedy algorithm. Since we always preferentially allocate resource to user with the maximum objective value and obtain local optimal solution, hence, a near optimal result of **SP3** can be achieved while avoiding the complexity of exhausting global optimal solution, as evidenced by the evaluation results in Section VI.

*3) Complexity:* Algorithm 1 jointly optimizes task splitting and computing resource assignment within $T$ slots and $Y$ PIoT users. Its complexity is $o(TYL_1)$, where $L_1$ is the number of iterations required. Suppose that $I$ iterations are needed to converge until no blocking pair exits in Algorithm 2. The number of swap-matching for each iteration requires $K^2$ operations at most. Thus, the complexity of Algorithm 2 is $o(ITK^2)$ [22]. Algorithm 3 optimizes the allocation of server side computing resources for $T$ time periods and $K$ UAVs, with a complexity of $o(TKL_3)$, and $L_3$ is iterations' number for server to find its preferential user. It is easy to calculate that the brute-force search needs $o(TM^K)$ iterations just for optimal channel reusing in each time slot.

## VI. SIMULATIONS RESULTS

We evaluation our solution with extensive simulation. We assume 1 HAPS, 4-12 UAVs, and several ground PIoT users distributed in a remote square area of 1000 m $\times$ 1000 m. Users are randomly distributed, and the hovering positions of the UAVs are optimized according to users' distribution [37], [38]. Each subchannel of HAPS can be reused by two UAVs and each UAV serves two UAUs via NOMA. The

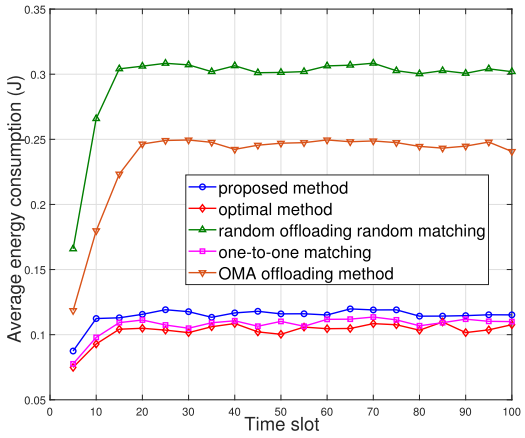


(a) Average energy consumption.

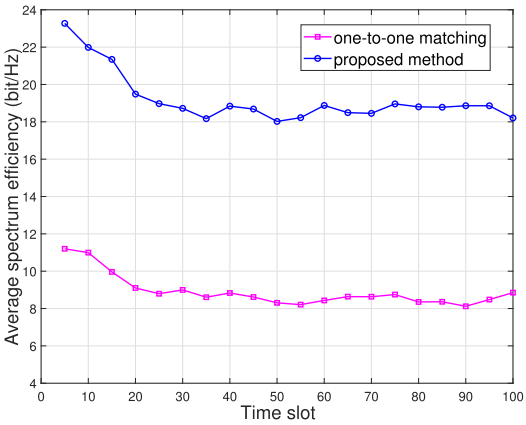


(b) Spectrum efficiency.

Fig. 2. Average energy consumption and spectrum efficiency.

number of arriving tasks $A_y(t)$ follows uniform distribution within [16.8, 25.2]$\times 10^4$ bits, and the maximum available computing resources $f_{y,max}(t)$, $f_{0,max}(t)$ and $f_{k,max}(t)$ are uniformly distributed within [1.6, 2.4], [264, 396], and [79.2, 118.8] GHz, respectively. The remaining parameters are presented in Table II.

Our proposed solution are compared with six benchmark approaches as follows.

1) *Random offloading random matching method*: Terminals randomly make offloading decisions, and UAVs randomly reuse subchannels.
2) *OMA offloading method*: Terminals occupy orthogonal subchannels for task offloading, and resource allocation is optimized by our approach.
3) *One-to-one matching method*: Each UAV is allowed to reuse mostly one subchannel.
4) *Full offloading method*: All tasks of each terminal are offloaded to the HAPS or its associated UAV, and power consumption is optimized by our approach.
5) *Full local computing method*: All tasks of each terminal are processed at local side, and power consumption is optimized by our approach.
6) *Optimal method*: **SP1** and **SP3** are solved by our proposed approach, while the channel reusing of **SP2** is realized by the brute-force search and its complexity is exponential, which is only feasible for small-scale problems.[1]

We optimize resource allocation and task offloading decision every $H$ slots, that is, when $t = r \times H + 1, r = 1, 2, 3, \ldots$ Algorithms 1,2,3 are executed for optimization, and for the rest of the time the task offloading action and channel allocation remain unchanged. In our simulation, $H = 5$ and we find that the actual calculation time is much less than $H \times \tau$. Therefore, the calculation cost of our proposed method is acceptable and is feasible in practice.

Fig. 2 (a) gives average power consumption over time. Results of average power consumption suggest that there is almost no difference among the proposed method, the one-to-one matching, and the optimal approach, while the proposed method outperforms random offloading random matching method and OMA offloading method by 148% and 99%, respectively. The reason is that, in one-to-one matching, there are more available orthogonal channels than that of many-to-one matching, so it is much easier to find a superior matching result. However, results of spectrum efficiency shown in Fig. 2 (b) show that our approach outperforms one-to-one matching method greatly. For instance, in $t = 35$ time slot, the performance of our proposed method is 96% of one-to-one matching in terms of energy consumption, however, spectrum efficiency (SE) of the proposed method outperforms one-to-one matching by 54%. The comparison results demonstrate that many-to-one matching has the outstanding overall performance in terms of both energy consumption and spectrum efficiency.

Fig. 3 (a)-(c) show the backlog of queue $Q_y^{loc}(t)$, $Q_y^{off}(t)$ and $G_{y,k}(t)$ over time. We are able to see the task backlog of the proposed approach is nearly the same as that of the optimal method, but is significantly lower than that in the random method, the full local computing method, and the full offloading method. The reason is that for the queue $Q_y^{loc}(t)$, the full local computing method has a large amount of local tasks due to no offloading strategy, while the random method lacks task offloading strategy and optimization of local resource allocation. For queues $Q_y^{off}(t)$ and $G_{y,k}(t)$, the full offloading method causes large backlog due to no task splitting, while the random method does not optimize the resource allocation at the aerial server side.

Fig. 4 (a)-(c) show the queue delay of $Q_y^{loc}(t)$, $Q_y^{off}(t)$ and $G_{y,k}(t)$ over time. It can be seen that the delay of the three queues all show a decreasing trend. From the numerical results, we can see that our proposed method reduces the queue delay $Q_y^{loc}(t)$, $Q_y^{off}(t)$ and $G_{y,k}(t)$ by 66.7%, 92.6%, and 82.7%, respectively, compared with the full local computing/full offloading. This is due to the compound effects of

[1] In our simulation, for comparing with the optimal method shown by Fig. 2 to Fig. 5, cluster's number alters from 2 to 4 while UAV's number varies from 4 to 8. The optimal method cannot return a result in reasonable time when the size of the network (e.g., the values of $K$ and $M$) becomes larger.

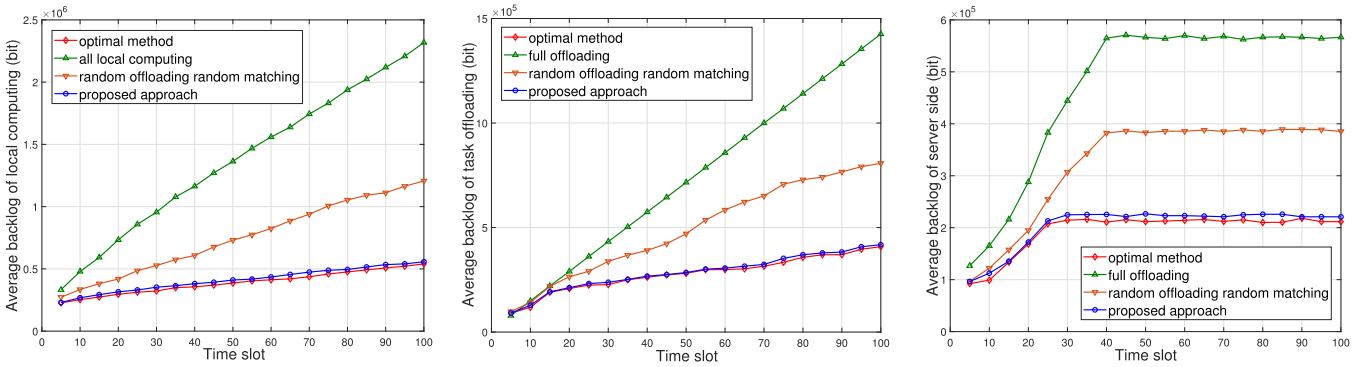


(a) Local computing $Q_y^{loc}(t)$. (b) Task offloading $Q_y^{off}(t)$. (c) Server side $G_{y,k}(t)$.

Fig. 3. Average backlog over time slot.

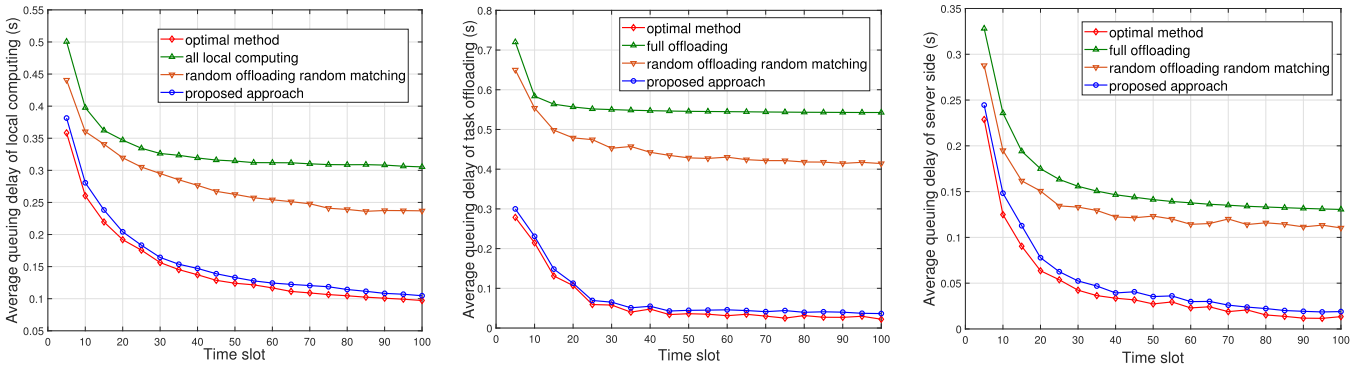


(a) Local computing $Q_y^{loc}(t)$. (b) Task offloading $Q_y^{off}(t)$. (c) Server side $G_{y,k}(t)$.

Fig. 4. Average queuing delay over time slot.

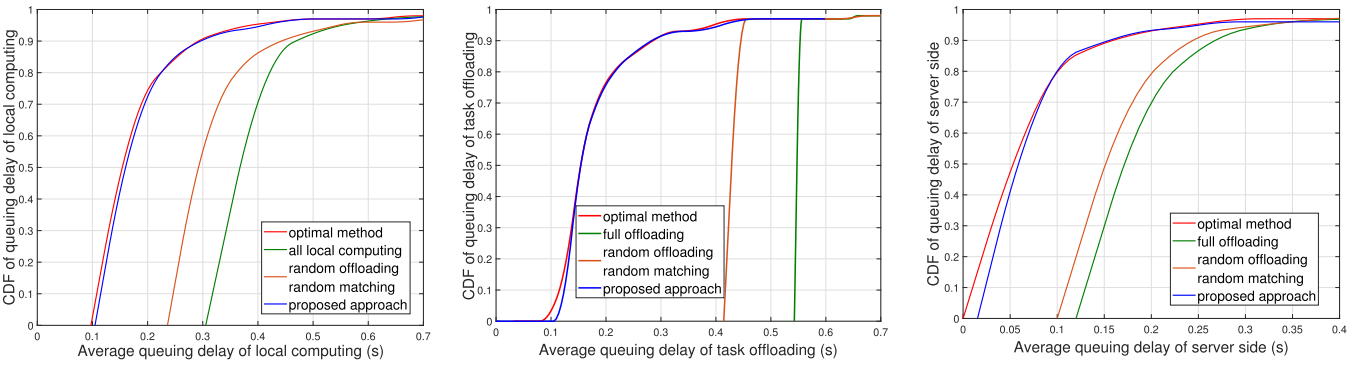


(a) Local computing $Q_y^{loc}(t)$. (b) Task offloading $Q_y^{off}(t)$. (c) Server side $G_{y,k}(t)$.

Fig. 5. CDF of queuing delay.

joint task splitting, computational and communication resource allocation, and queue-awareness.

Fig. 5 (a)-(c) show the CDF of queue delay of $Q_y^{loc}(t)$, $Q_y^{off}(t)$ and $G_{y,k}(t)$. Results verify that overall queue delay of our approach is much lower compared with other benchmark approaches and can quickly converge to a value that satisfies the constraints.

Fig. 6 (a) shows the impact of local computing capability $f_{y,max}$ on the average energy consumption. It can be seen that energy consumption of all local computing and random offloading random matching grows sharply. The reason is that all computing resources are used to process the large local queuing backlogs. However, the energy consumption of our proposed method is comparatively low due to queue-awareness, and more tasks can be offloaded. Fig. 6 (b) shows the average energy consumption versus edge computing capability $f_{k,max}$. Results also verify that our proposed method has superior performance than other methods and is near optimal.

Figs. 7 and 8 show the CDF and the total energy consumption versus swap operations' number. Results suggest

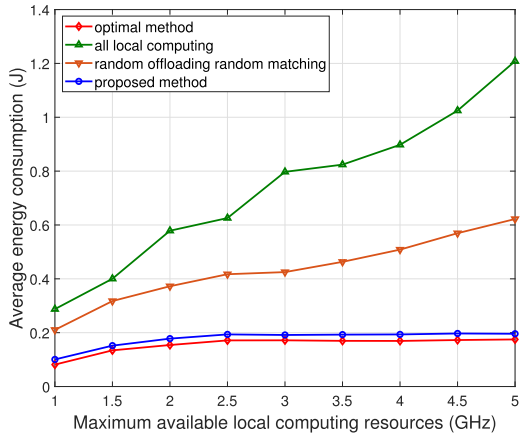


(a) Local computing capability $f_{y,max}$.

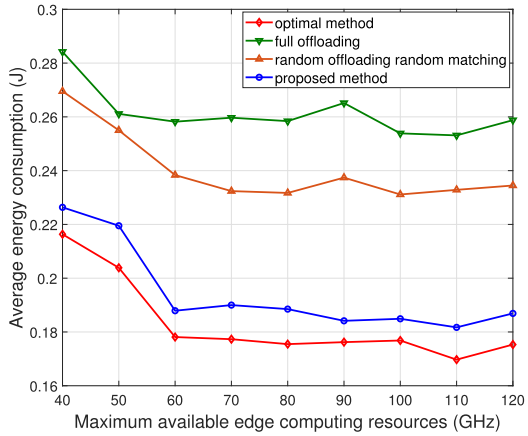


(b) Edge computing capability $f_{k,max}$

Fig. 6. Impacts of computing resource on the energy consumption.

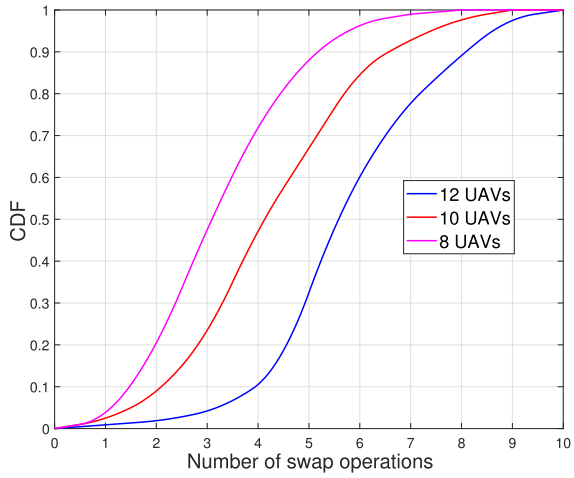


Fig. 7. CDF of number of swap operations.

that increasing UAVs' number causes more swap operations. We can also find when there are 12 UAVs, the proposed approach converges to stable matching with optimal total energy consumption of 5.82J in at most 10 swap operations. Moreover, increasing the number of UAVs leads to more PIoT

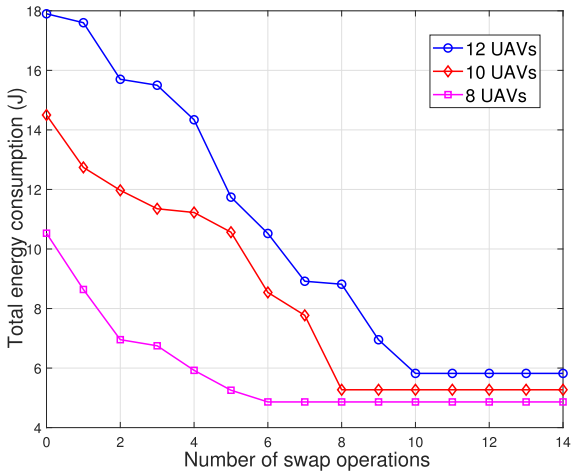


Fig. 8. Total energy consumption versus number of swap operations.

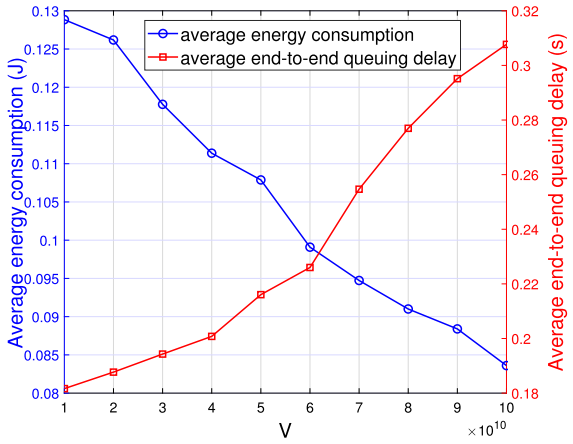


Fig. 9. Impact of V.

users, thus, the system consumes more total energy. This also verifies our algorithms' effectiveness.

Fig. 9 shows the impact of $V$. With the increment of $V$, the average energy consumption decreases and the queue delay increases, indicating that our method pays more attention to energy consumption reduction than the queue delay decrements. Specifically, the average energy consumption reduces by $34.4\%$, and the queue delay increases by $41.6\%$ when $V$ increases from $10^{10}$ to $10^{11}$. It demonstrates that our method can obtain good balance between power consumption and queue delay.

## VII. Conclusion

In this paper, we investigated the energy minimization queue-aware task offloading and resource allocation problem for PAGIC HetNets. We leveraged Lyapunov optimization for transforming our origin issue to three subproblems, i.e., task splitting and local computational resource assignment for the user side, channel reusing and task offloading optimization, and edge resource assignment for aerial server side. Accordingly, we developed TSCRA, EMCAM$^2$ and EMGERA algorithms to solve the three subproblems step by

step. We also analyze convergence, optimality, and complexity of our approach. Simulation results reveal that the proposed approach can achieve outstanding overall performance with low complexity in terms of power consumption, spectrum efficiency, task backlog, and queuing delay.

## REFERENCES


[1] X. Fang, S. Misra, G. Xue, and D. Yang, "Smart grid—The new and improved power grid: A survey," *IEEE Commun. Surveys Tuts.*, vol. 14, no. 4, pp. 944–980, Qua. 2012.

[2] G. Bedi, G. K. Venayagamoorthy, R. Singh, R. R. Brooks, and K.-C. Wang, "Review of Internet of Things (IoT) in electric power and energy systems," *IEEE Internet Things J.*, vol. 5, no. 2, pp. 847–870, Apr. 2018.

[3] M. Tariq, M. Ali, F. Naeem, and H. Poor, "Vulnerability assessment of 6G-enabled smart grid cyber–physical systems," *IEEE Internet Things J.*, vol. 8, no. 7, pp. 5468–5475, Apr. 2021.

[4] Z. Zhang *et al.*, "6G wireless networks: Vision, requirements, architecture, and key technologies," *IEEE Veh. Technol. Mag.*, vol. 14, no. 3, pp. 28–41, Sep. 2019.

[5] J. Liu, X. Zhao, P. Qin, S. Geng, and S. Meng, "Joint dynamic task offloading and resource scheduling for WPT enabled space-air-ground power Internet of Things," *IEEE Trans. Netw. Sci. Eng.*, vol. 9, no. 2, pp. 660–677, Mar. 2022.

[6] H. Hidayat, M. A. Wibisono, R. Fikri, and S. M. Ulfa, "Error pointing correction system implemented in the air balloon communication system," in *Proc. 12th Int. Conf. Telecommun. Syst., Services, Appl. (TSSA)*, Oct. 2018, pp. 1–6.

[7] Haryono, "Balloon trajectory: Monitoring, prediction, and analysis," in *Proc. Int. Conf. Inf. Commun. Technol. (ICOIACT)*, Jul. 2019, pp. 709–714.

[8] Z. Na, Y. Liu, J. Shi, C. Liu, and Z. Gao, "UAV-supported clustered NOMA for 6G-enabled Internet of Things: Trajectory planning and resource allocation," *IEEE Internet Things J.*, vol. 8, no. 20, pp. 15041–15048, Oct. 2021.

[9] *Iridium Official Website*. Accessed: 2022. [Online]. Available: https://www.iridium.com/

[10] H. Su *et al.*, "Nonorthogonal interleave-grid multiple access scheme for industrial Internet of Things in 5G network," *IEEE Trans. Ind. Informat.*, vol. 14, no. 12, pp. 5436–5446, Dec. 2018.

[11] Z. Q. Al-Abbasi and D. K. C. So, "Resource allocation in non-orthogonal and hybrid multiple access system with proportional rate constraint," *IEEE Trans. Wireless Commun.*, vol. 16, no. 10, pp. 6309–6320, Oct. 2017.

[12] F. Fang, J. Cheng, and Z. Ding, "Joint energy efficient subchannel and power optimization for a downlink NOMA heterogeneous network," *IEEE Trans. Veh. Technol.*, vol. 68, no. 2, pp. 1351–1364, Feb. 2019.

[13] H. Liao, Z. Zhou, and X. Zhao, "Learning-based queue-aware task offloading and resource allocation for space–air–ground-integrated power IoT," *IEEE Internet Things J.*, vol. 8, no. 7, pp. 5250–5263, Apr. 2021.

[14] X. Chen, D. W. K. Ng, W. Yu, E. G. Larsson, N. Al-Dhahir, and R. Schober, "Massive access for 5G and beyond," *IEEE J. Sel. Areas Commun.*, vol. 39, no. 3, pp. 615–637, Mar. 2021.

[15] X. Wang, L. T. Yang, D. Meng, M. Dong, K. Ota, and H. Wang, "Multi-UAV cooperative localization for marine targets based on weighted subspace fitting in SAGIN environment," *IEEE Internet Things J.*, vol. 9, no. 8, pp. 5708–5718, Apr. 2022, doi: 10.1109/JIOT.2021.3066504.

[16] S. Yu, X. Gong, Q. Shi, X. Wang, and X. Chen, "EC-SAGINs: Edge computing-enhanced space–air–ground integrated networks for internet of vehicles," *IEEE Internet Things J.*, vol. 9, no. 8, pp. 5742–5754, Apr. 2022, doi: 10.1109/JIOT.2021.3052542.

[17] C. Zhou *et al.*, "Deep reinforcement learning for delay-oriented IoT task scheduling in SAGIN," *IEEE Trans. Wireless Commun.*, vol. 20, no. 2, pp. 911–925, Feb. 2021.

[18] B. Shang and L. Liu, "Mobile-edge computing in the sky: Energy optimization for air–ground integrated networks," *IEEE Internet Things J.*, vol. 7, no. 8, pp. 7443–7456, Aug. 2020.

[19] Y. Sun, D. Xu, D. W. K. Ng, L. Dai, and R. Schober, "Optimal 3D-trajectory design and resource allocation for solar-powered UAV communication systems," *IEEE Trans. Commun.*, vol. 67, no. 6, pp. 4281–4298, Jun. 2019.

[20] T. X. Tran and D. Pompili, "Joint task offloading and resource allocation for multi-server mobile-edge computing networks," *IEEE Trans. Veh. Technol.*, vol. 68, no. 1, pp. 856–868, Jan. 2019.

[21] F. Guo, H. Zhang, H. Ji, X. Li, and V. C. M. Leung, "An efficient computation offloading management scheme in the densely deployed small cell networks with mobile edge computing," *IEEE/ACM Trans. Netw.*, vol. 26, no. 6, pp. 2651–2664, Dec. 2018.

[22] C. Xu, G. Zheng, and X. Zhao, "Energy-minimization task offloading and resource allocation for mobile edge computing in NOMA heterogeneous networks," *IEEE Trans. Veh. Technol.*, vol. 69, no. 12, pp. 16001–16016, Dec. 2020.

[23] A. M. Seid, G. O. Boateng, B. Mareri, G. Sun, and W. Jiang, "Multi-agent DRL for task offloading and resource allocation in multi-UAV enabled IoT edge network," *IEEE Trans. Netw. Service Manage.*, vol. 18, no. 4, pp. 4531–4547, Dec. 2021.

[24] Z. Li, Y. Wang, M. Liu, R. Sun, Y. Chen, J. Yuan, and J. Li, "Energy efficient resource allocation for UAV-assisted space-air-ground internet of remote things networks," *IEEE Access*, vol. 7, pp. 145348–145362, 2019.

[25] Y. Wu, B. Shi, L. P. Qian, F. Hou, J. Cai, and X. S. Shen, "Energy-efficient multi-task multi-access computation offloading via NOMA transmission for IoTs," *IEEE Trans. Ind. Informat.*, vol. 16, no. 7, pp. 4811–4822, Jul. 2020.

[26] R. Li, P. Hong, K. Xue, M. Zhang, and T. Yang, "Resource allocation for uplink NOMA-based D2D communication in energy harvesting scenario: A two-stage game approach," *IEEE Trans. Wireless Commun.*, vol. 21, no. 2, pp. 976–990, Feb. 2022.

[27] Z. Ding, P. Fan, and H. V. Poor, "Impact of non-orthogonal multiple access on the offloading of mobile edge computing," *IEEE Trans. Commun.*, vol. 67, no. 1, pp. 375–390, Jan. 2019.

[28] W. U. Khan, F. Jameel, X. Li, M. Bilal, and T. A. Tsiftsis, "Joint spectrum and energy optimization of NOMA-enabled small-cell networks with QoS guarantee," *IEEE Trans. Veh. Technol.*, vol. 70, no. 8, pp. 8337–8342, Aug. 2021.

[29] Q. Zhang, K. Luo, W. Wang, and T. Jiang, "Joint C-OMA and C-NOMA wireless backhaul scheduling in heterogeneous ultra dense networks," *IEEE Trans. Wireless Commun.*, vol. 19, no. 2, pp. 874–887, Feb. 2020.

[30] A. Shahini and N. Ansari, "NOMA aided narrowband IoT for machine type communications with user clustering," *IEEE Internet Things J.*, vol. 6, no. 4, pp. 7183–7191, Aug. 2019.

[31] K. Wang, W. Liang, Y. Yuan, Y. Liu, Z. Ma, and Z. Ding, "User clustering and power allocation for hybrid non-orthogonal multiple access systems," *IEEE Trans. Veh. Technol.*, vol. 68, no. 12, pp. 12052–12065, Oct. 2019.

[32] J. Ding and J. Cai, "Two-side coalitional matching approach for joint MIMO-NOMA clustering and BS selection in multi-cell MIMO-NOMA systems," *IEEE Trans. Wireless Commun.*, vol. 19, no. 3, pp. 2006–2021, Mar. 2020.

[33] Y. Gu, W. Saad, M. Bennis, M. Debbah, and Z. Han, "Matching theory for future wireless networks: Fundamentals and applications," *IEEE Commun. Mag.*, vol. 53, no. 5, pp. 52–59, May 2015.

[34] Y. Yuan, T. Yang, Y. Hu, H. Feng, and B. Hu, "Two-timescale resource allocation for cooperative D2D communication: A matching game approach," *IEEE Trans. Veh. Technol.*, vol. 70, no. 1, pp. 543–557, Jan. 2021.

[35] D. Chen *et al.*, "Matching-theory-based low-latency scheme for multitask federated learning in MEC networks," *IEEE Internet Things J.*, vol. 8, no. 14, pp. 11415–11426, Jul. 2021.

[36] P. Qin, Y. Fu, X. Feng, X. Zhao, S. Wang, and Z. Zhou, "Energy-efficient resource allocation for parked-cars-based cellular-V2V heterogeneous networks," *IEEE Internet Things J.*, vol. 9, no. 4, pp. 3046–3061, Feb. 2022.

[37] W. Huang *et al.*, "Joint power, altitude, location and bandwidth optimization for UAV with underlaid D2D communications," *IEEE Wireless Commun. Lett.*, vol. 8, no. 2, pp. 524–527, Apr. 2019.

[38] P. Qin, Y. Zhu, X. Zhao, X. Feng, J. Liu, and Z. Zhou, "Joint 3D-location planning and resource allocation for XAPS-enabled C-NOMA in 6G heterogeneous Internet of Things," *IEEE Trans. Veh. Technol.*, vol. 70, no. 10, pp. 10594–10609, Oct. 2021.

[39] N. Cheng, F. Lyu, W. Quan, C. Zhou, H. He, W. Shi, and X. Shen, "Space/aerial-assisted computing offloading for IoT applications: A learning-based approach," *IEEE J. Sel. Areas Commun.*, vol. 37, no. 5, pp. 1117–1129, May 2019.

[40] S. M. R. Islam, N. Avazov, O. A. Dobre, and K.-S. Kwak, "Power-domain non-orthogonal multiple access (NOMA) in 5G systems: Potentials and challenges," *IEEE Commun. Surveys Tuts.*, vol. 19, no. 2, pp. 721–742, 2nd Quart., 2017.

[41] C. F. Liu, M. Bennis, M. Debbah, and H. V. Poor, "Dynamic task offloading and resource allocation for ultra-reliable low-latency edge computing," *IEEE Trans. Commun.*, vol. 67, no. 6, pp. 4132–4150, Feb. 2019.
[42] Y. Mao, J. Zhang, S. H. Song, and K. B. Letaief, "Power-delay tradeoff in multi-user mobile-edge computing systems," in *Proc. IEEE Global Commun. Conf. (GLOBECOM)*, Washington, DC, USA, Dec. 2016, pp. 1–6.
[43] W. Bao, H. Chen, Y. Li, and B. Vucetic, "Joint rate control and power allocation for non-orthogonal multiple access systems," *IEEE J. Sel. Areas Commun.*, vol. 35, no. 12, pp. 2798–2811, Dec. 2017.
[44] M. Neely, *Stochastic Network Optimization With Application to Communication and Queueing Systems*. San Rafael, CA, USA: Morgan & Claypool, 2010.
[45] S.-Y. Jung, J. Hong, and K. Nam, "Current minimizing torque control of the IPMSM using Ferrari's method," *IEEE Trans. Power Electron.*, vol. 28, no. 12, pp. 5603–5617, Dec. 2013.
[46] E. Bodine-Baron, C. Lee, A. Chong, B. Hassibi, and A. Wierman, "Peer effects and stability in matching markets," in *Proc. 4th Int. Symp. Algorithmic Game Theory*, Oct. 2011, pp. 117–129.

**Peng Qin** (Member, IEEE) received the B.S. and Ph.D. degrees from the Huazhong University of Science and Technology, Wuhan, China, in 2009 and 2014, respectively. From 2012 to 2013, he was a Visiting Scholar with the University of Victoria, Victoria, BC, Canada. He is currently an Associate Professor with the School of Electrical and Electronic Engineering, North China Electric Power University. His research interests include resource allocation in the Internet of Things, smart grid communications, space air ground integrated networks, and vehicular networks. He was a recipient of the International Communications Signal Processing and Systems Conference Best Paper Award and the International Conference on Artificial Intelligence in China Best Paper Award in 2019, 2020, and 2021, respectively.

**Yang Fu** is currently pursuing the B.S. degree with the School of Electrical and Electronic Engineering, North China Electric Power University. His research interests include resource allocation in smart grid communications, space air ground integrated networks, vehicular networks, and the Internet of Things.

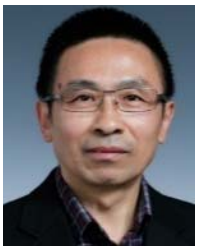

**Xiongwen Zhao** (Senior Member, IEEE) received the Ph.D. degree from the Helsinki University of Technology, Finland, in 2002. From 2004 to 2011, he was with Elektrobit Corporation. He is currently a Chair Professor of information and communications engineering with North China Electric Power University and responsible for the projects supported by the National Science Foundation of China and the Double First Class Construction Project by the Ministry of Education. He is a fellow of the Chinese Institute of Electronics. He was a recipient of the IEEE VTS Neal Shepherd Memorial Best Propagation Paper Award, the IEEE ISAPE Best Paper Award, and the IWCMC Best Paper Award in 2014, 2018, and 2019, respectively. He has served as the TPC co-chair and a keynote speaker for numerous international conferences. He is an Associate Editor of *IET Communications*.

**Kui Wu** (Senior Member, IEEE) received the B.Sc. and M.Sc. degrees in computer science from Wuhan University, China, in 1990 and 1993, respectively, and the Ph.D. degree in computing science from the University of Alberta, Canada, in 2002. In 2002, he joined the Department of Computer Science, University of Victoria, Canada, where he is currently a Full Professor. His research interests include network performance analysis, mobile and wireless networks, and network performance evaluation.

**Jiayan Liu** received the B.S. degree from North China Electric Power University in 2019, where she is currently pursuing the Ph.D. degree with the School of Electrical and Electronic Engineering. Her research interests include space air ground integrated networks, network resource optimization, and the Power Internet of Things.

**Miao Wang** received the B.S. degree from Shandong Normal University in 2020. She is currently pursuing the M.Sc. degree with the School of Electrical and Electronic Engineering, North China Electric Power University. Her research interests include space-air-ground integrated networks, network resource optimization, and the Power Internet of Things.